

Tunable Eigenvector-Based Centralities for Multiplex and Temporal Networks *

Dane Taylor[†], Mason A. Porter[‡], and Peter J. Mucha[§]

Abstract. Characterizing the importances (i.e., centralities) of nodes in social, biological, information and technological networks is a core topic for the network-science and data-science communities. In this paper, we present a linear-algebraic framework that generalizes eigenvector-based centralities—including PageRank and hub/authority scores—to provide a common framework for two popular classes of multilayer networks: multiplex networks with layers encoding different types of relationships and temporal networks in which the relationships change in time. Our approach involves the study of *joint, marginal, and conditional supracentralities* that can be obtained from the dominant eigenvector of a *supracentrality matrix* [Taylor et al., 2017], which couples centrality matrices that are associated with the individual network layers. We extend this prior work (which was restricted to temporal networks with layers that are coupled by undirected, adjacent-in-time coupling) by allowing the layers to be coupled through a (possibly asymmetric) *interlayer adjacency matrix* $\tilde{\mathbf{A}}$ in which each entry $\tilde{A}_{tt'} > 0$ gives the coupling between layers t and t' . Our framework provides a unifying foundation for centrality analysis of multiplex and/or temporal networks and reveals a complicated dependency of the supracentralities on the topology of interlayer coupling, as encoded by $\tilde{\mathbf{A}}$. We also scale $\tilde{\mathbf{A}}$ by an interlayer coupling strength $\omega \geq 0$ and develop singular perturbation theory for the limits of weak ($\omega \rightarrow 0^+$) and strong coupling ($\omega \rightarrow \infty$), which reveals an interesting dependence on the dominant left and right eigenvectors of $\tilde{\mathbf{A}}$. We provide additional theoretical and practical insights by applying the framework to two empirical data sets: a multiplex network representation of airline transportation in Europe, and a temporal network encoding the graduation and hiring of mathematicians at U.S. colleges and universities.

Key words. Network science, Multilayer networks, Data integration, Ranking systems, Perturbation theory

AMS subject classifications. 91D30, 05C81, 94C15, 05C82, 15A18

1. Introduction. Quantifying the importance of entities in a network representation of a data set is an essential feature of many internet search engines [11, 32, 58, 75], ranking algorithms for sports teams and athletes [12, 15, 90], targeted social-network marketing schemes [51], investigations of fragility in infrastructures [39, 42], quantitative research on the impact of research papers and scientists [30], research on the influence of judicial and legislative documents [31, 59], and the identification of novel drug targets in biological systems [48]. In the most common (and simplest) type of network, called a “graph” or “monolayer network”, a node represents an entity (e.g., webpages, persons, documents, proteins, etc.), and an edge encodes a relationship between a pair of entities. *Centrality analysis*, quantifying node and

*We thank Deryl DeFord, Tina Eliassi-Rad, Des Higham, Christine Klymko, Marianne McKenzie, Scott Pauls, and Michael Schaub for fruitful conversations. DT was supported by the Simons Foundation, Award #578333. PJM was supported by the Eunice Kennedy Shriver National Institute of Child Health & Human Development of the National Institutes of Health under Award Number R01HD075712 and by the James S. McDonnell Foundation 21st Century Science Initiative - Complex Systems Scholar Award grant #220020315. The content is solely the responsibility of the authors and does not necessarily reflect the views of any of the funding agencies.

[†]Department of Mathematics, University at Buffalo, State University of New York, Buffalo, NY 14260, USA

[‡]Department of Mathematics, University of California, Los Angeles, CA 90095, USA

[§]Carolina Center for Interdisciplinary Applied Mathematics, Department of Mathematics and Department of Applied Physical Sciences, University of North Carolina, Chapel Hill, NC 27599, USA

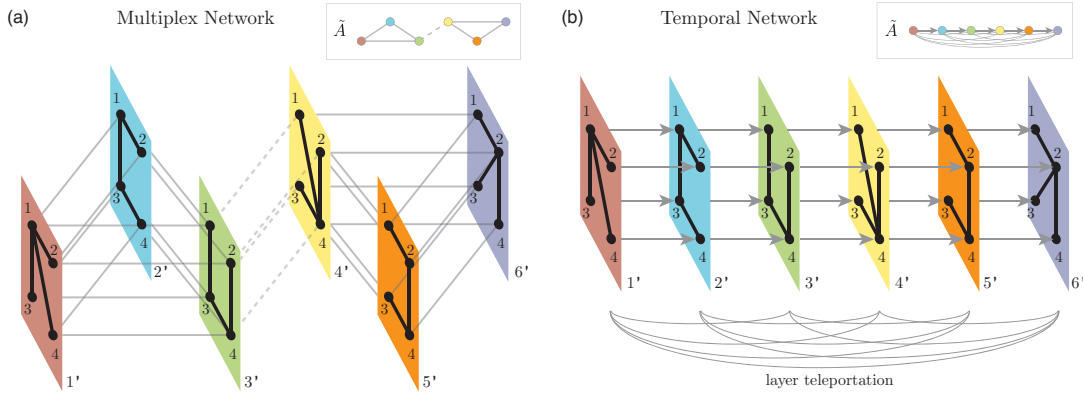


Figure 1. Schematics of two types of multilayer networks. (a) A *multiplex network*, in which layers are coupled categorically. (b) A *multiplex representation of a discrete-time temporal network*, where we couple the sequence of layers through a directed (time-respecting) chain with layer teleportation (see Sec. 5.2). Each inset depicts the interlayer-coupling topology that we encode using an interlayer adjacency matrix \hat{A} . We assume that the interlayer couplings are “diagonal” and “uniform” (see Sec. 2.2), and we take their weights to be $\omega \geq 0$. As shown in panels (a) and (b), the interlayer coupling can be undirected or directed.

edge importances (and, more generally, subgraph importances), has been developed across numerous domains, including sociology, mathematics, computer science, and physics [19, 32, 58, 72].

Scholars have developed increasingly comprehensive network representations to help with data integration [53, 74], including the generalization of graphs to *multilayer networks* [8, 18, 53, 79] and of centrality measures for multilayer and temporal networks [2, 26, 37, 38, 41, 52, 60, 68, 77, 87, 89, 91, 92, 96, 97, 102, 111, 112]. Multilayer network centralities have been used in the study of diverse applications, including social networks [14, 17, 41, 63, 64], transportation systems [22, 47, 98, 107], economic systems [5, 23, 24], neuroscience [6, 20, 47, 113], and signal processing of geological time series [62]. Moreover, many techniques in centrality analysis are closely connected to the study of various dynamical processes on multilayer networks, including random walks [25, 34, 41, 73], information spreading [17, 85], and congestion [22].

We consider two types of multilayer networks (see Fig. 1): *multiplex networks*, in which layers represent different types of relationships; and *temporal networks*, in which layers represent different points or periods in time. We further develop the mathematical framework of *supracentrality* matrices, which we developed previously [102] to generalize eigenvector-based centralities — e.g., PageRank [11, 32, 75], eigenvector centrality [10], and hub and authority scores [55] — to multilayer representations of discrete-time temporal networks. The approach involves coupling together centrality matrices associated with the individual layers into a larger supracentrality matrix and studying its dominant eigenvector to obtain *joint, marginal, and conditional centralities* (see Sec. 3.2) to generally quantify the importances of nodes, layers or *node-layer pairs*. In this article, we extend the supracentrality framework to multiplex networks, which integrate multiple data sets by coupling them as layers in a single multilayer network.

Generalizing centrality measures to multiplex networks and temporal networks are both

active areas of research [8, 18, 43, 44, 53] (see our discussion in Sec. 2.3), and the supracentrality framework that we discuss is relevant for both of these threads.¹ Our original formulation of supracentrality in [102] focused on temporal networks, assuming a particular type of multilayer representation with adjacent-in-time coupling. We now extend supracentrality matrices to a broader class of multilayer networks by coupling layers via an interlayer adjacency matrix $\tilde{\mathbf{A}}$, where $\tilde{A}_{tt'} \geq 0$ encodes the (possibly asymmetric) coupling between layers t and t' . We assume “diagonal” interlayer coupling (see Sec. 2.2 and [53]) in that we only connect together representations of the same entity (i.e., nodes) in different layers. We also assume the interlayer coupling is “uniform” in that all edges between layers t and t' have the same edge weight $\omega \tilde{A}_{tt'} \geq 0$. The value of ω determines how strongly the layers influence each other. We will show that the choices for $\tilde{\mathbf{A}}$ and ω significantly affect supracentralities and are useful “tuning knobs” to consider in calculating and interpreting supracentralities.

To gain theoretical insight into the effects of $\tilde{\mathbf{A}}$ and ω , we develop singular perturbation theory to analyze the dominant eigenspace of supracentrality matrices in the limits of weak ($\omega \rightarrow 0^+$) and strong coupling ($\omega \rightarrow \infty$). We show these limits implement, respectively, layer decoupling and a type of layer aggregation (i.e., data fusion). There are many scenarios in which one couples matrices into a larger “supramatrix” — e.g., the detection of multilayer community structure using a supramodularity matrix [69, 110] and the study of random walks and diffusion on multilayer networks via supraLaplacian matrices [34, 83] — and our perturbative approach reveals insights about the utility of matrix coupling as a general technique for multimodal data integration. Specifically, the singular perturbation theory presented in Sec. 4 makes no explicit assumption that the block-diagonal matrices are centrality matrices, and so our results characterize the dominant eigenspace for layer-coupled matrices studied in other applications, including even applications that are unrelated to networks.

Our new results in Sec. 4 characterize decoupling and aggregation limits for the dominant eigenspace for uniformly and diagonally-coupled matrices. In the strong-coupling limit, the dominant eigenvector of such a supramatrix is determined by the dominant eigenvector of a matrix that one can obtain as a weighted average of the coupled matrices, with weights that depend on the dominant eigenvectors of $\tilde{\mathbf{A}}$. By contrast, in the weak-coupling limit, the dominant eigenvector is determined by the dominant eigenvector of a matrix that depends on $\tilde{\mathbf{A}}$, as well as the spectral radii and dominant eigenvectors of the matrices that are being coupled. A key factor for determining the decoupling limit is whether the matrices have identical or different spectral radii; for the latter scenario, we identify and characterize an eigenvector-localization phenomenon by which one or more layers dominate the decoupling limit. Finally, we note that the layer-aggregation and decoupling limits we study are similar to, but notably different from, existing results for supraLaplacian matrices [34, 94] (which assume $\tilde{\mathbf{A}}$ must be symmetric, for example).

We illustrate our framework with applications to two empirical, multimodal network data sets. First, we study the importances of European airports in a multiplex network in which layers represent different airlines [13]. We study layer-coupled eigenvector centralities and find that centralities in the weak-coupling limit are dominated by the Ryanair layer, which has

¹In principle, one can also use supracentrality matrices, of higher dimensionality, to study networks that are *both* multiplex and temporal, but we do not study such an example in this paper.

the most edges and whose adjacency matrix has the largest spectral radius. For intermediate coupling strengths, we observe a centrality “boost” (i.e., increase relative to the other nodes’ centralities) for airports that are central to *both* the Ryanair layer and the network associated with the aggregation of the network layers (i.e., the summation of the layers’ adjacency matrices). We study these phenomena by comparing marginal node centralities to the nodes’ intralayer and total degrees (which quantify, respectively, the number of edges in each layer and the total number of edges across layers). The second data set is based on the Mathematical Genealogy Project [82, 100] and is a temporal network that describes the graduation and hiring of mathematicians at mathematical-science Ph.D. programs in the United States [102]. Extending our previous study [102], we now explore the effects of causality by implementing time-directed interlayer coupling along with *layer teleportation* (see Fig. 1(b)), which we define analogously to *node teleportation* in PageRank [32]. Similar to previous findings for causality-respecting centralities [28, 36], this approach preferentially boosts the centralities of node-layer pairs whose edges occur earlier in time (which allows them to causally influence more nodes). Specifically, this phenomenon manifests as a boost in marginal layer centrality for older time layers. Our numerical experiments highlight the importance of exploring a diverse set of interlayer-coupling topologies $\tilde{\mathbf{A}}$ and strengths ω to identify application-appropriate parameter choices.

Our paper is organized as follows. In Sec. 2, we present background information on eigenvector-based centralities, multiplex and temporal networks, and generalizing centralities for such networks. In Sec. 3, we present our supracentrality framework. In Sec. 4, we analyze the weak- and strong-coupling limits. In Sec. 5, we study the empirical data sets. We conclude in Sec. 6 and give the proofs for our main mathematical results in appendices. Extended numerical investigations are given in a Supplementary Material.

2. Background Information. We present background information on eigenvector-based centralities in Sec. 2.1, multiplex and temporal networks in Sec. 2.2, and extensions of centrality for multiplex and temporal networks in Sec. 2.3.

2.1. Eigenvector-Based Centrality Measures. We start with a definition.

Definition 2.1 (Monolayer Network). *Let $\mathcal{G}(\mathcal{V}, \mathcal{E})$ denote a monolayer (i.e., single-layer) network with nodes $\mathcal{V} = \{1, 2, \dots, N\}$ and a set $\mathcal{E} \subset \mathcal{V} \times \mathcal{V} \times \mathbb{R}_+$ of positively-weighted edges, where $(i, j, w_{ij}) \in \mathcal{E}$ if and only if there exists an edge from i to j with weight w_{ij} . We also encode this network (which is a weighted graph) by an $N \times N$ adjacency matrix \mathbf{A} with entries $A_{ij} = w_{ij}$ if $(i, j, w_{ij}) \in \mathcal{E}$ and $A_{ij} = 0$ otherwise.*

One of the most popular approaches for quantifying the importances of nodes \mathcal{V} in a network is to calculate the dominant eigenvector of a network-related matrix and interpret the eigenvector’s entries as a proxy for importance [32, 72].²

Definition 2.2 (Eigenvector-Based Centrality Measure). *Let $\mathbf{C} = C(\mathbf{A})$ denote a “centrality matrix” obtained via some function $C : \mathbb{R}^{N \times N} \mapsto \mathbb{R}^{N \times N}$ of adjacency matrix \mathbf{A} for network*

²There are also other centralities, such as Katz centrality, that involve eigenvectors but are not equal to the entry of a dominant eigenvector [72].

$\mathcal{G}(\mathcal{V}, \mathcal{E})$. Consider the right dominant eigenvector \mathbf{u} , the solution of

$$(2.1) \quad \mathbf{C}\mathbf{u} = \lambda_{\max}\mathbf{u},$$

where $\lambda_{\max} \in \mathbb{R}$ is the largest eigenvalue of \mathbf{C} . Each entry u_i specifies the eigenvector-based centrality associated with the function C for node $i \in \mathcal{V}$.

Different choices for $C(\mathbf{A})$ yield different notions of centrality, and some are more useful than others. The following are among the most popular eigenvector-based centralities.

Definition 2.3 (Eigenvector Centrality [10]). With the choice $\mathbf{C}^{(EC)} = \mathbf{A}$, Eq. (2.1) yields eigenvector centralities $\{u_i^{(EC)}\}$.

Definition 2.4 (Hub and Authority Scores [55]). With the choices $\mathbf{C}^{(HS)} = \mathbf{A}\mathbf{A}^T$ and $\mathbf{C}^{(AS)} = \mathbf{A}^T\mathbf{A}$, Eq. (2.1) yields hub scores $\{u_i^{(HS)}\}$ and authority scores $\{u_i^{(AS)}\}$, respectively.

Remark 2.1. Note that hub scores and authority scores are, respectively, the dominant left and right singular vectors of \mathbf{A} .

Definition 2.5 (PageRank [32,75]). Consider the choice $\mathbf{C}^{(PR)} = \gamma\mathbf{A}\mathbf{D}^{-1} + (1-\gamma)N^{-1}\mathbf{1}\mathbf{1}^T$, where \mathbf{D} is a diagonal matrix that encodes the node degrees (i.e., $D_{ij} = \delta_{ij} \sum_j A_{ij}^T$), $\gamma \in [0, 1]$ is a “node teleportation” parameter (we assume $\gamma = 0.85$ unless we specify otherwise), and $\mathbf{1}$ is a length- N vector of ones (giving $\mathbf{1}\mathbf{1}^T$ as an $N \times N$ matrix of ones). Using this choice in Eq. (2.1), we obtain PageRank centralities $\{u_i^{(PR)}\}$.

Remark 2.2. It is also common to compute PageRank centralities from a left eigenvector [32]. In the present paper, we use a right-eigenvector formulation to be consistent with the other eigenvector-based centralities. One can recover the other formulation by taking the transpose of Eq. (2.1).

Remark 2.3. There are other possible teleportation strategies for PageRank, such as local bias and emphasis of other features [32]. In such cases, one employs vectors other than $\mathbf{1}$ for the teleportation term.

In most applications, it is important to choose the function C to ensure centralities are unique and strictly positive. The following two theorems are used widely to guarantee this.

Theorem 2.6 (Perron–Frobenius Theorem for Nonnegative Matrices [4]). Let $\mathbf{C} \in \mathbb{R}^{N \times N}$ denote an irreducible square matrix with nonnegative entries. It then follows that \mathbf{C} has a simple largest positive eigenvalue λ_{\max} and that its left and right eigenvectors are positive and unique. Moreover, if \mathbf{C} is aperiodic (i.e., $\mathbf{C} \neq \mathbf{C}^k$ for any $k > 1$), then λ_{\max} is a dominant eigenvalue: $|\lambda_i| < \lambda_{\max}$ for $i \neq \operatorname{argmax}_{i \in \mathcal{V}} |\lambda_i|$.

Theorem 2.7 (Strong Connectivity Implies Irreducibility [4]). Consider the (possibly weighted and directed) network associated with a nonnegative square matrix \mathbf{C} . If the associated network is strongly connected (i.e., there exists a path from any node to any node), then \mathbf{C} is irreducible.

Thus, one typically seeks a centrality matrix \mathbf{C} that is irreducible (or equivalently, a matrix such that its associated network defined by the weighted edges $\{(i, j, C_{ij})\}$ is strongly connected). Ensuring irreducibility is an important consideration when introducing new types of centrality (including ones with both positive and negative edges [27]). For example, the

term $(1 - \alpha)N^{-1}\mathbf{1}\mathbf{1}^T$ in Definition 2.5 implies $\mathbf{C}^{(PR)}$ is positive (i.e., $C_{ij}^{(PR)} > 0$ for every $i, j \in \mathcal{V}$), which ensures $\mathbf{C}^{(PR)}$ is irreducible regardless of whether the network with adjacency matrix \mathbf{A} is strongly connected [32].

Before continuing, we highlight an eigenvector-based centrality measure that uses both the left and right eigenvectors and therefore does not exactly fit Definition 2.2. The *dynamical importance* of a node is defined in terms of the change of the leading eigenvalue of \mathbf{A} under removal of that node from the network [86] (see also [106]). In practice, as shown in [86], one can approximate dynamical importance to first order (provided one does not lose strong connectivity when removing the node) with an expression that depends on the leading right and left eigenvectors of \mathbf{A} . Indeed, other eigenvector-based centralities involving two or more eigenvectors obtained by analyzing matrix perturbations have been developed to cater to particular applications including disease spreading [101, 103], percolation [86, 104], and synchronization of dynamical systems [105]. Such works explore perturbations of dynamical systems on networks are related to eigenvalue and eigenvector elasticities [35, 49, 50].

2.2. Multiplex and Temporal Networks. The different layers in a multilayer network can encode different types of connections and/or interacting systems [53], including interconnected critical infrastructures [40], categories of social ties [57], networks at different instances in time [109], and many others. By considering the various possibilities for interactions between nodes within and across layers, one can obtain a taxonomy for different types of multilayer networks [53]. We focus on two popular situations: *multiplex networks*, in which different layers represent different types of interactions; and *temporal networks*, in which layers represent different time instances or time periods. We provide formal definitions that are salient for these last two situations.

Definition 2.8 (Uniformly and Diagonally Coupled Multiplex Network). Let $\mathcal{G}(\mathcal{V}, \{\mathcal{E}^{(t)}\}, \tilde{\mathcal{E}})$ denote a multilayer network with nodes $\mathcal{V} = \{1, \dots, N\}$ and T layers, with interactions between node-layer pairs encoded by the sets $\{\mathcal{E}^{(t)}\}$ of weighted edges, where $(i, j, w_{ij}^t) \in \mathcal{E}^{(t)}$ if and only if there is an edge (i, j) with weight w_{ij}^t in layer t . The set $\tilde{\mathcal{E}} = \{(s, t, \tilde{w}_{st})\}$ encodes the topology and weights for coupling separate instances of the same node between pairs of layers $(s, t) \in \{1, \dots, T\} \times \{1, \dots, T\}$. One can equivalently encode a multiplex network as a set of adjacency matrices $\{\mathbf{A}^{(t)}\}$ such that $A_{ij}^{(t)} = w_{ij}^t$ if $(i, j, w_{ij}^t) \in \mathcal{E}^{(t)}$ and $A_{ij}^{(t)} = 0$ otherwise, along with an interlayer-adjacency matrix $\tilde{\mathbf{A}}$ with components $\tilde{A}_{st} = \tilde{w}_{st}$ if $(s, t, \tilde{w}_{st}) \in \tilde{\mathcal{E}}$ and $\tilde{A}_{ij}^{(t)} = 0$ otherwise.

See Fig. 1(a) for a pedagogical example of a small multiplex network. The multiplex coupling in Definition 2.8 is “diagonal” because we only allow coupling between a node in one layer and that same node in other layers, and it is “uniform” because the coupling between two layers is identical for all nodes in those two layers. Our choice to represent interlayer couplings via $\tilde{\mathbf{A}}$ is a generalization of the special, but commonly assumed, case where the interlayer edge weights are identical for all layer pairs, i.e., $\tilde{w}_{st} = \omega$ for any s and t . Although there are many other coupling strategies [9, 53], we focus on uniform and diagonal coupling because it is one of the simplest and most popular coupling schemes, and at the same time the interlayer-adjacency matrix $\tilde{\mathbf{A}}$ allows for a great deal of flexibility and fine tuning. Moreover, as we will describe in Sec. 3, these restrictions impose matrix symmetries that we will exploit

to derive results for when the layers are coupled either very weakly or very strongly.

We use a similar multilayer network representation to study temporal networks.

Definition 2.9 (Discrete-Time Temporal Network). *A discrete-time temporal network consists of nodes $\mathcal{V} = \{1, \dots, N\}$ and a sequence of network layers. We denote it either as $\mathcal{G}(\mathcal{V}, \{\mathcal{E}^{(t)}\})$ or by a sequence of adjacency matrices $\{\mathbf{A}^{(t)}\}$ such that $A_{ij}^{(t)} = w_{ij}^t$ if $(i, j, w_{ij}^t) \in \mathcal{E}^{(t)}$ and $A_{ij}^{(t)} = 0$ otherwise. A discrete-time temporal network may also include coupling between layers.*

Note that Definition 2.9 makes no explicit assumptions about how the layers are coupled. That is, a discrete-time temporal network consists of a set of nodes and an ordered set of layers. It is common, however, for investigations of temporal network to introduce coupling between time layers, representing them (as we do) as a multiplex network with an interlayer coupling that respects time.

Finally, we note that because there are N nodes and T layers, it is convenient for both temporal and multiplex networks to refer to a given node i in a given layer t using the *node-layer pair* (i, t) .

2.3. Extensions of Centrality for Multiplex and Temporal Networks. There has been a recent explosion of research on centrality measures for multilayer networks [18, 53]. Much of this work is related to work on generalizing network properties such as node degree [7, 21, 64, 98] and shortest paths, with the latter leading to generalizations of betweenness centrality [14, 63, 92, 93] and closeness centrality [64, 93]. Of particular relevance to the present paper are generalizations of eigenvector-based centralities to multiplex networks, including for eigenvector centrality [7, 21, 23, 24, 91], hub and authority scores [56, 84, 95, 107], and PageRank [25, 41, 73]. These extensions have employed various strategies, several of which we briefly indicate.

One strategy is to represent a multiplex network as a tensor and use tensor decompositions [56]. Another strategy is to define a system of centrality dependencies in which high-centrality elements (nodes, layers, and so on) connect to other high-centrality elements, and one simultaneously solves for multiple types of centrality [84, 95, 107] as a fixed-point solution of the system of (possibly nonlinear) dependencies. For example, [84] and [107] defined centralities for both nodes and layers such that high-ranked layers contain high-ranked nodes and high-ranked nodes are in high-ranked layers. In a third strategy, which is the one that most closely resembles our present approach, one constructs a *supramatrix* of size $NT \times NT$ for N nodes and T layers, such that the centralities of node-layer pairs $\{(i, t)\}$ are given by the dominant eigenvector of the supramatrix. For example, [23, 24, 88, 91] constructed a supramatrix by using the Khatri–Rao matrix product between a matrix that encodes interlayer connections and a block matrix that has the layers’ adjacency matrices as columns. Finally, another approach involves computing one or more centralities independently for each layer and using consensus ranking [80].

Turning our attention to temporal extensions to centrality, we refer the reader to discussions in [102] and [61]. To add to these lists, we briefly highlight contributions that appeared recently or otherwise were not mentioned in [102]. Arrigo and Higham [3] introduced a method to efficiently estimate temporal communicability (a generalization of Katz centrality), which was been applied to a variety of applications, including neuroscience [65] and disease

spreading [16, 66]. Huang and Yu [45] extended a measure called dynamic-sensitive centrality to temporal networks. References [29, 46, 81] introduced variants of eigenvector centrality for temporal networks. We highlight [29] in particular because it explored connections between continuous and discrete-time calculations of temporal centralities. Nathan et al. [70] introduced an efficient algorithm for computing exponential centrality for streaming graphs. Although methods for streaming and continuous-time networks are important (see, e.g., [1]), we restrict our present attention to discrete-time temporal networks in an effort to further bridge the literatures on temporal networks and multiplex networks.

In Sec. 3, we introduce a new construction for a supramatrix that is based on a Kronecker product, generalizing our previous work [102], where we introduced a supracentrality framework for temporal networks and assumed adjacent in time coupling (i.e., $A_{ij}^{(t)} = 1$ if and only if $|i - j| = 1$ and $A_{ij}^{(t)} = 0$ otherwise). Our new formulation introduces an interlayer-adjacency matrix $\mathbf{A}^{(t)}$ allowing the framework to flexibly cater to multiplex and/or temporal networks. We note, however, that there are other multilayer representations of temporal networks. One popular approach is to connect each node-layer pair (i, t) to $\{(j, t + 1)\}$ for $j \in \{j : A_{ij}^{(t)} \neq 0\}$, yielding a supra-adjacency matrix with identity matrices on the block diagonal and the layers' adjacency matrices on the off-diagonal blocks just above the diagonal blocks. These interlayer edges are nondiagonal, connecting nodes in one layer to different nodes in the next layer. This formulation, connected mathematically [28] to matrix-iteration-based centrality measures for temporal networks [36–38], has been used to study time-dependent functional brain networks [108].

Finally, we emphasize that one could of course choose to study multiplex and temporal networks without interlayer coupling, by independently considering each layer in isolation.

Table 1

Summary of our mathematical notation.

Typeface	Class	Dimensionality
\mathbb{M}	matrix	$NT \times NT$
\mathbf{M}	matrix	$N \times N$
\mathbf{M}	matrix	$T \times T$
\mathbf{w}	vector	$NT \times 1$
\mathbf{v}	vector	$N \times 1$
\mathbf{v}	vector	$T \times 1$
M_{ij}	scalar	1
v_i	scalar	1

3. Supracentrality Framework for Multiplex/Temporal Networks. We now present a supracentrality framework that provides a common mathematical foundation for eigenvector-based centralities for multiplex and temporal networks. In Sec. 3.1, we define supracentrality matrices. In Sec. 3.2, we define joint, marginal, and conditional centralities; and we prove their uniqueness and positivity under certain conditions. In Sec. 3.3, we provide a pedagogical example to illustrate these concepts. We summarize our mathematical notation in Table 1.

3.1. Supracentrality Matrices. We first define a supracentrality matrix for networks that are multiplex and/or temporal, which generalizes the definition in [102].

Definition 3.1 (Supracentrality Matrix). Let $\{\mathbf{C}^{(t)}\}$ denote a set of T centrality matrices for a multilayer network whose layers have a common set $\mathcal{V} = \{1, \dots, N\}$ of nodes, and suppose that $C_{ij}^{(t)} \geq 0$. Let $\tilde{\mathbf{A}}$ with $\tilde{A}_{ij} \geq 0$ denote a $T \times T$ interlayer adjacency matrix encoding the interlayer couplings. We define a family of supracentrality matrices $\mathbb{C}(\omega)$, parameterized by interlayer-coupling strength $\omega \geq 0$, taking the form

$$(3.1) \quad \begin{aligned} \mathbb{C}(\omega) &= \hat{\mathbf{C}} + \omega \hat{\mathbf{A}} \\ &= \begin{bmatrix} \mathbf{C}^{(1)} & \mathbf{0} & \mathbf{0} & \dots \\ \mathbf{0} & \mathbf{C}^{(2)} & \mathbf{0} & \dots \\ \mathbf{0} & \mathbf{0} & \mathbf{C}^{(3)} & \dots \\ \vdots & \vdots & \ddots & \ddots \end{bmatrix} + \omega \begin{bmatrix} \tilde{A}_{11}\mathbf{I} & \tilde{A}_{12}\mathbf{I} & \tilde{A}_{13}\mathbf{I} & \dots \\ \tilde{A}_{21}\mathbf{I} & \tilde{A}_{22}\mathbf{I} & \tilde{A}_{23}\mathbf{I} & \dots \\ \tilde{A}_{31}\mathbf{I} & \tilde{A}_{32} & \tilde{A}_{33}\mathbf{I} & \dots \\ \vdots & \vdots & \vdots & \ddots \end{bmatrix}, \end{aligned}$$

where $\hat{\mathbf{C}} = \text{diag}[\mathbf{C}^{(1)}, \dots, \mathbf{C}^{(T)}]$ and $\hat{\mathbf{A}} = \tilde{\mathbf{A}} \otimes \mathbf{I}$ denotes the Kronecker product of $\tilde{\mathbf{A}}$ and \mathbf{I} .

Remark 3.1. For layer t , matrix $\mathbf{C}^{(t)}$ can represent any matrix whose dominant eigenvector is of interest. We, of course, will focus on centrality matrices such as those associated with eigenvector centrality (see Definition 2.3), hub and authority scores (see Definition 2.4), or PageRank (see Definition 2.5). Also, note that one could scale each $\mathbf{C}^{(t)}$ by a layer-specific weight, which has been observed to benefit multilayer community detection [76] and layer-averaged clique detection [71]. Such weighting can easily be incorporated into Eq. (3.1) by redefining the centrality matrices $\{\mathbf{C}^{(t)}\}$ to include the weights.

The supracentrality matrix $\mathbb{C}(\omega)$ of size $NT \times NT$ encodes the effects of two distinct types of connections: the layer-specific centrality entries $\{C_{ij}^{(t)}\}$ in the diagonal blocks relate centralities between nodes within layer t , while entries in the off-diagonal blocks encode coupling between layers. Note that the form $\hat{\mathbf{A}} = \tilde{\mathbf{A}} \otimes \mathbf{I}$ implements uniform and diagonal coupling: the matrix \mathbf{I} implements diagonal coupling, and any two layers t and t' are uniformly coupled since all interlayer edges between them have identical weight, $w\tilde{A}_{tt'}$. The choice of undirected, adjacent-in-time interlayer coupling—that is, $\tilde{A}_{tt'} = 1$ if $|t - t'| = 1$ and $\tilde{A}_{tt'} = 0$ otherwise—recovers the supracentrality matrix studied in [102]. Generalizing [102], we introduce in this paper the interlayer adjacency $\tilde{\mathbf{A}}$, which is an important methodological contribution and allows one to implement a wide variety of *interlayer coupling topologies*. In the context of multiplex networks, we hypothesize that different choices for $\tilde{\mathbf{A}}$ will have varying benefits. In the context of temporal networks, we will study (Sec. 5.2) the effects of letting $\tilde{\mathbf{A}}$ encode a directed, time-respecting chain with “layer teleportation” (see Eq. (5.1)), obtaining supracentrality results that contrast with those in [102].

3.2. Joint, Marginal, and Conditional Centralities. The defining feature of eigenvector-based centrality measures is that one computes and studies a dominant eigenvector of a centrality matrix. Therefore, we study the right dominant eigenvalue equation

$$(3.2) \quad \mathbb{C}(\omega)\mathbf{v}(\omega) = \lambda_{\max}(\omega)\mathbf{v}(\omega),$$

where we interpret entries in the right dominant eigenvector $\mathfrak{v}(\omega)$ as centrality measures for the node-layer pairs $\{(i, t)\}$. Following [102], we use the concepts of “joint”, “marginal”, and “conditional” centrality to develop our understanding of the importances of nodes and/or layers from the computed $\mathfrak{v}(\omega)$ values.

Definition 3.2 (Joint Centrality of a Node-Layer Pair [102]). Let $\mathbb{C}(\omega)$ denote a supracentrality matrix given by Definition 3.1, and let $\mathfrak{v}(\omega)$ denote its dominant right eigenvector. We encode the joint centrality of node i in layer t via the $N \times T$ matrix $\mathbf{W}(\omega)$ with entries

$$(3.3) \quad W_{it}(\omega) = \mathfrak{v}_{N(t-1)+i}(\omega).$$

Remark 3.2. We refer to $W_{it}(\omega)$ as a “joint centrality” because it reflects the importance both of node i and of layer t .

Definition 3.3 (Marginal Centralities of Nodes and Layers [102]). Let $\mathbf{W}(\omega)$ encode the joint centralities given by Definition 3.2. We define the marginal layer centrality (MLC) and marginal node centrality (MNC), respectively, by

$$(3.4) \quad x_t(\omega) = \sum_i W_{it}(\omega), \quad \hat{x}_i(\omega) = \sum_t W_{it}(\omega).$$

Definition 3.4 (Conditional Centralities of Nodes and Layers [102]). Let $\{W_{it}(\omega)\}$ denote the joint centralities given by Definition 3.2, and let $\{x_t(\omega)\}$ and $\{\hat{x}_i(\omega)\}$ respectively denote the marginal node and layer centralities given by Definition 3.3. We define the conditional centralities of nodes and layers by

$$(3.5) \quad Z_{it}(\omega) = W_{it}(\omega)/x_t(\omega), \quad \hat{Z}_{it}(\omega) = W_{it}(\omega)/\hat{x}_i(\omega),$$

where $Z_{it}(\omega)$ gives the centrality of node i conditioned on layer t , and $\hat{Z}_{it}(\omega)$ gives the centrality of layer t conditioned on node i .

Note that $Z_{it}(\omega)$ indicates the importance of node i relative to other nodes in layer t , in contrast with the joint node-layer centrality $W_{it}(\omega)$, which reflects the importance of node-layer pair (i, t) relative to all node-layer pairs.

We now present a new theorem that ensures the uniqueness and positivity of the supracentralities defined above.

Theorem 3.5 (Uniqueness and Positivity of Supracentralities). Let $\mathbb{C}(\omega)$ denote a supracentrality matrix given by Eq. (3.1), suppose that $\tilde{\mathbf{A}}$ is an adjacency matrix for a strongly connected graph, and suppose that the summation $\sum_t \mathbf{C}^{(t)}$ is an irreducible nonnegative matrix. It then follows that $\mathbb{C}(\omega)$ is irreducible, nonnegative, and has a simple largest positive eigenvalue $\lambda_{\max}(\omega)$ with corresponding left and right eigenvectors $\mathfrak{u}(\omega)$ and $\mathfrak{v}(\omega)$, respectively, that are unique and consist of positive entries. Moreover, the centralities $\{W_{it}(\omega)\}$, $\{x_i(\omega)\}$, $\{\hat{x}_t(\omega)\}$, $\{Z_{it}(\omega)\}$, and $\{\hat{Z}_{it}(\omega)\}$ are positive and well-defined. If, in addition, $\mathbb{C}(\omega)$ is aperiodic, then $\lambda_{\max}(\omega)$ is a unique dominant eigenvalue.

Proof. See Appendix A. ■

3.3. Pedagogical Example. In Fig. 2, we illustrate the concepts of joint and marginal centralities for the network in Fig. 1(a). The multiplex network has $N = 4$ nodes and $T = 6$ layers, and we study the interlayer-adjacency matrix $\tilde{\mathbf{A}}$ visualized in the inset of Fig. 1(a). Specifically, we set $\tilde{A}_{tt'} = 1$ for all depicted interlayer couplings, except for the coupling of layers 3 and 4, for which we set $\tilde{A}_{34} = \tilde{A}_{43} = 0.01$. With this weighting, the interlayer-coupling network associated with $\tilde{\mathbf{A}}$ has two natural communities of densely-connected nodes.

		layer index						
		1	2	3	4	5	6	MNC
node index	1	0.1615	0.1578	0.1554	0.1930	0.1923	0.1925	1.0524
	2	0.0961	0.0959	0.0958	0.3008	0.3064	0.3123	1.2072
	3	0.1468	0.1504	0.1511	0.1930	0.1923	0.1925	1.0260
	4	0.1188	0.1185	0.1225	0.3131	0.3068	0.3009	1.2807
MLC		0.5231	0.5226	0.5248	0.9999	0.9978	0.9981	

Figure 2. Joint node-layer centralities $\{W_{it}(\omega)\}$ given by Definition 3.2 (white cells), with corresponding marginal layer centralities (MLC) $\{x_t(\omega)\}$ and marginal node centralities (MNC) $\{\hat{x}_i(\omega)\}$ given by Definition 3.3 (gray cells), for the multiplex network in Fig. 1(a). These results reflect diagonally and uniformly coupled eigenvector centralities in which the layers' centrality matrices are given by Definition 2.3 with $\omega = 1$.

For this experiment and others below, we typically find that conditional centrality provides the most useful insights. In Fig. 3(a), we plot the conditional centralities $\{Z_{it}(\omega)\}$ of node-layers for three different choices of ω . These choices represent three centrality regimes that we observe by exploring centralities across a range of ω values, which we illustrate in Fig. 3(b). In the top two panels of Fig. 3(b), we plot the MNC and MLC values versus ω . In the bottom panel, we quantify the sensitivity of the joint and conditional centralities to perturbations of ω . Specifically, we consider ω in the interval $[10^{-2}, 10^4]$ discretized by $\omega_s = 10^{-2+0.2s}$ for $s \in \{0, \dots, 30\}$. We plot the stepwise magnitudes of the change, $\|\mathbf{W}(\omega_s) - \mathbf{W}(\omega_{s-1})\|_F$, of the joint centralities and the change, $\|\mathbf{Z}(\omega_s) - \mathbf{Z}(\omega_{s-1})\|_F$, of the conditional centralities, where $\|\cdot\|_F$ denotes the Frobenius norm. We identify three regimes in which the conditional centralities are robust (the shaded regions in the bottom panel of Fig. 3(b)). Interestingly, the ranges of ω in which $\mathbf{Z}(\omega)$ is robust do not coincide perfectly with those for $\mathbf{W}(\omega)$. We focus on robust values of $\mathbf{Z}(\omega)$, because we generally find conditional centrality to provide the most interpretable and insightful results (see also Secs. 3.2 and 5 in [102]).

We summarize these three regimes as follows:

- **Weak-Coupling Regime.** The top panel of Fig. 3(a), at $\omega = 10^{-2}$, represents a regime in which conditional centralities resemble the centralities of uncoupled layers as $\omega \rightarrow 0^+$. In this example, we observe the conditional centralities correlate strongly with nodes' intralayer degrees, $d_i^{(t)} = \sum_j A_{ij}^{(t)}$. Specifically, as indicated by the horizontal dashed lines, the conditional centralities approximately equal one of three values: $Z_{it} \approx 0.3656$ when $d_i^{(t)} = 3$; $Z_{it} \approx 0.3096$ when $d_i^{(t)} = 2$; and $Z_{it} \approx 0.2021$ when

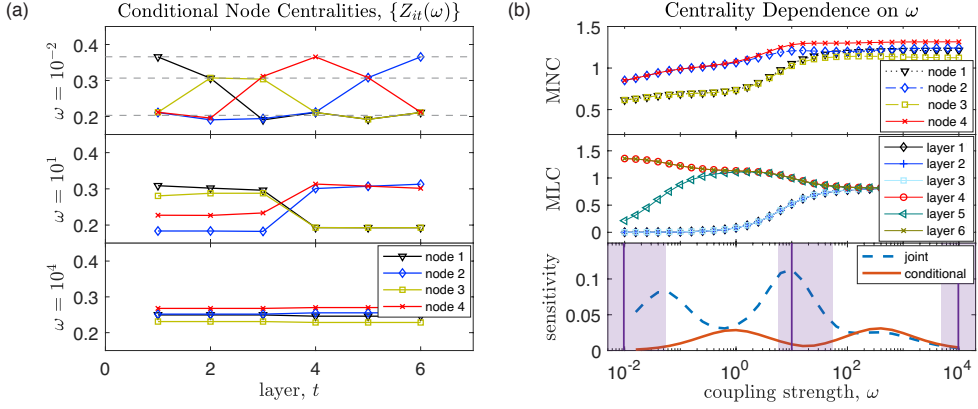


Figure 3. Eigenvector centralities (see Definition 2.3) for the uniformly and diagonally coupled multilayer network with interlayer-adjacency matrix $\tilde{\mathbf{A}}$ given by $\tilde{A}_{tt'} = 1$ for the coupled layers in Fig. 1(a), except for $\tilde{A}_{34} = \tilde{A}_{43} = 0.01$. (a) Conditional node centralities $\{Z_{it}(\omega)\}$ versus t for $\omega \in \{10^{-2}, 10, 10^4\}$. Horizontal dashed lines in the top panel highlight that $\{Z_{it}(\omega)\}$ values correlate with intralayer node degrees $d_i^{(t)} = \sum_j A_{ij}^{(t)}$: $Z_{it}(\omega) \approx 0.3656$ when $d_i^{(t)} = 3$; $Z_{it}(\omega) \approx 0.3096$ when $d_i^{(t)} = 2$; and $Z_{it}(\omega) \approx 0.2021$ when $d_i^{(t)} = 1$. (b) MNC and MLC versus ω on the interval $[10^{-2}, 10^4]$ discretized by $\omega_s = 10^{-2+0.2s}$ for $s \in \{0, \dots, 30\}$. The bottom panel depicts a measure for the sensitivity of centralities with respect to ω . We plot the stepwise magnitude of change, $\|\mathbf{W}(\omega_s) - \mathbf{W}(\omega_{s-1})\|_F$, for the joint centralities and the change, $\|\mathbf{Z}(\omega_s) - \mathbf{Z}(\omega_{s-1})\|_F$, for the conditional centralities. The shaded regions visually highlight three separate regimes in which $\mathbf{Z}(\omega)$ is more robust to the perturbation of ω . The vertical lines indicate the ω values from panel (a).

$d_i^{(t)} = 1$. We analyze the $\omega \rightarrow 0^+$ limit in Sec. 4.1.

- **Strong-Coupling Regime.** The bottom panel of Fig. 3(a), at $\omega = 10^4$, represents a regime in which the conditional centralities approach the centralities of a layer-aggregated centrality matrix as $\omega \rightarrow \infty$. In this regime, the conditional centralities limit to a value $Z_{it} \rightarrow \alpha_i$ for each i that is constant across the layers. We analyze the $\omega \rightarrow \infty$ limit in Sec. 4.2.
- **Intermediate-Coupling Regime.** The middle panel of Fig. 3(a), at $\omega = 10$, represents an intermediate regime. We typically study this regime numerically. We observe two subsets of Z_{it} conditional centrality values: those for layers $t \in \{1, 2, 3\}$ are very similar to each other, while those for layers $t \in \{4, 5, 6\}$ are also similar to each other. This pattern arises directly from the layer-coupling scheme in Fig. 1(a), where these two sets of layers correspond to two communities for the interlayer-adjacency matrix. (Recall that the coupling between layers 3 and 4 is 100 times weaker than the other couplings.) In Sec. SM1 of the Supplementary Material, we show that this robust intermediate regime vanishes as one increases the coupling weight between layers 3 and 4.

Note that we classify regimes by considering if the observed supracentralities are correlated with those of either asymptotic limit (i.e., either $\omega \rightarrow 0^+$ or $\omega \rightarrow \infty$) or not correlated with either limit. The intermediate regime arises from an interplay between the topologies and edge weights of both the layers and the interlayer couplings, so these multilayer centralities provide insights that cannot be observed by studying the network layers in isolation or in aggregate.

This example also illustrates that it is important to explore various coupling strengths ω as well as various interlayer-adjacency matrices $\tilde{\mathbf{A}}$ to identify supracentralities that are appropriate for a given application. Our MATLAB code that computes supracentralities and reproduces the above experiment is available at [99].

4. Limiting Behavior for Weak and Strong Coupling. We develop singular perturbation expansions to analyze the limiting behaviors of Eq. (3.2) when the interlayer-coupling strength ω is very small (i.e., layer decoupling) or very large (i.e., layer aggregation). These results provide insights into our supracentrality framework and can aid in the selection of appropriate parameter choices.

4.1. Layer Decoupling in the Weak-Coupling Limit. We first give a general result for the $\omega \rightarrow 0^+$ limit of all eigenvalues and eigenvectors of $\mathbb{C}(\omega)$. We highlight that this limit was not studied in our previous work [102].

Theorem 4.1 (Layer Decoupling as $\omega \rightarrow 0^+$). *Assume that each layer's $N \times N$ centrality matrix $\mathbf{C}^{(t)}$ is diagonalizable, let $\{\mu_i^{(t)}\}$ denote its N eigenvalues, and let $\{\mathbf{u}^{(i,t)}\}$ and $\{\mathbf{v}^{(i,t)}\}$ denote the corresponding left and right eigenvectors. Let $\mathbb{C}(\omega)$ denote a supracentrality matrix given by Eq. (3.1), let $\{\lambda_n(\omega)\}$ denote its NT eigenvalues, with corresponding left eigenvectors $\mathbf{u}^{(n)}(\omega)$ and right eigenvectors $\mathbf{v}^{(n)}(\omega)$. In the limit $\omega \rightarrow 0^+$, we have $\mathbb{C}(\omega) \rightarrow \hat{\mathbb{C}} = \text{diag}[\mathbf{C}^{(1)}, \dots, \mathbf{C}^{(T)}]$ and $\{\lambda_n(\omega)\} \rightarrow \cup_t \{\mu_i^{(t)}\}$. The limiting associated left and right eigenvectors $\mathbf{u}^{(n)}(\omega)$ and $\mathbf{v}^{(n)}(\omega)$ are determined by functions of the eigenvectors $\{\mathbf{u}^{(i,t)}\}$ and $\{\mathbf{v}^{(i,t)}\}$, respectively; and there are two cases, which depend on the sets of eigenvalues.*

- (1) *When the eigenvalues $\{\mu_i^{(t)}\}$ of $\mathbf{C}^{(t)}$ are simple and differ across layers — that is, when $\{\mu_i^{(t)}\} \cap \{\mu_i^{(t')}\} = \emptyset$ for $t \neq t'$ — there is a one-to-one correspondence between $\{\mu_i^{(t)}\}$ and $\{\lambda_n(0^+)\}$. The limiting eigenvalues of $\mathbb{C}(0^+)$ are then simple and correspond to eigenvectors $\mathbf{u}^{(n)}(\omega) \rightarrow \mathbf{u}^{(i,t)} = \mathbf{e}^{(t)} \otimes \mathbf{u}^{(i,t)}$ and $\mathbf{v}^{(n)}(\omega) \rightarrow \mathbf{v}^{(i,t)} = \mathbf{e}^{(t)} \otimes \mathbf{v}^{(i,t)}$. Here, $\mathbf{e}^{(t)}$ is a length- T unit vector consisting of zeros except the t -th entry, which is one, so that the vectors $\mathbf{u}^{(i,t)}$ and $\mathbf{v}^{(i,t)}$ consist of zeros except in the t -th blocks, which consist of $\mathbf{u}^{(i,t)}$ or $\mathbf{v}^{(i,t)}$.*
- (2) *When there are repeated eigenvalues, such that there exists a set $\mathcal{P} = \{(i,t) | \mu_i^{(t)} = \lambda_n\}$ with cardinality $P = |\mathcal{P}|$, each unique eigenvalue λ_n of $\mathbb{C}(0)$ has a P -dimensional eigenspace that is spanned by the left and right eigenvectors, $\{\mathbf{u}^{(i,t)}\}$ and $\{\mathbf{v}^{(i,t)}\}$, associated with λ_n .*

Proof. See Appendix B. ■

We now present a main result for the right dominant eigenvector of $\mathbb{C}(\omega)$.

Theorem 4.2 (Weak-Coupling Limit of Dominant Eigenvector). *Let $\mathbf{u}^{(1)}(\omega)$ and $\mathbf{v}^{(1)}(\omega)$ denote the dominant left and right eigenvectors of a supracentrality matrix under the assumptions of Thms. 3.5 and 4.1, and let $\mathcal{P} = \{t : \mu_1^{(t)} = \lambda_{\max}(0)\}$ denote the set of indices associated with the eigenvalues of $\mathbf{C}^{(t)}$ that equal the largest eigenvalue $\lambda_{\max}(0)$ of $\mathbb{C}(0)$. We assume that each layer's dominant eigenvalue $\mu_1^{(t)}$ is simple. It then follows that the $\omega \rightarrow 0^+$ limits of*

$\mathbf{u}^{(1)}(\omega)$ and $\mathbf{v}^{(1)}(\omega)$ are

$$(4.1) \quad \mathbf{v}^{(1)}(\omega) \rightarrow \sum_{t \in \mathcal{P}} \alpha_t \mathbf{v}^{(1,t)}, \quad \mathbf{u}^{(1)}(\omega) \rightarrow \sum_{t \in \mathcal{P}} \beta_t \mathbf{u}^{(1,t)},$$

where the vectors $\boldsymbol{\alpha} = [\alpha_1, \dots, \alpha_T]^T$ and $\boldsymbol{\beta} = [\beta_1, \dots, \beta_T]^T$, which have nonnegative entries that satisfy $\sum_t \alpha_t^2 = \sum_t \beta_t^2 = 1$, are unique solutions to

$$(4.2) \quad \mathbf{X}\boldsymbol{\alpha} = \lambda_1 \boldsymbol{\alpha}, \quad \mathbf{X}^T \boldsymbol{\beta} = \lambda_1 \boldsymbol{\beta},$$

where λ_1 is an eigenvalue that needs to be determined and the entries of \mathbf{X} are

$$(4.3) \quad X_{tt'} = \tilde{A}_{t,t'} \frac{\langle \mathbf{u}^{(1,t)}, \mathbf{v}^{(1,t')} \rangle}{\langle \mathbf{u}^{(1,t)}, \mathbf{v}^{(1,t)} \rangle} \chi(t) \chi(t'),$$

where $\chi(t) = \sum_{t' \in \mathcal{P}} \delta_{tt'}$ is an indicator function, with $\chi(t) = 1$ if $t \in \mathcal{P}$ and $\chi(t) = 0$ otherwise.

Proof. See Appendix C. ■

It is worth considering Thm. 4.2 under various restrictions on the centrality matrices, which gives rise to three corollaries. When the layers' centrality matrices all have the same spectral radius, as is the case for PageRank matrices (i.e., since they correspond to transition matrices of Markov chains) or if one rescales the centrality matrices to have the same spectral radius, then the limiting behavior simplifies as described by the following corollary.

Corollary 4.3 (Weak-Coupling Limit for Spectral-Radii-Equivalent Centrality Matrices). *Under the assumptions of Thm. 4.2 and assuming that all centrality matrices have the same spectral radius (i.e., $\lambda_{\max} = \mu_1^{(t)}$ for all t), then $\mathcal{P} = \{1, \dots, T\}$, $\chi(t) = 1$, and Eq. (4.3) takes the form*

$$(4.4) \quad X_{tt'} = \tilde{A}_{t,t'} \frac{\langle \mathbf{u}^{(1,t)}, \mathbf{v}^{(1,t')} \rangle}{\langle \mathbf{u}^{(1,t)}, \mathbf{v}^{(1,t)} \rangle}.$$

When the layers' centrality matrices are symmetric, which is the case for hub/authority matrices and symmetric adjacency matrices, then the limiting behavior simplifies as described next.

Corollary 4.4 (Weak-Coupling Limit for Symmetric Centrality Matrices). *Under the assumptions of Thm. 4.2 and assuming that all centrality matrices are symmetric, then $\mathbf{u}^{(1,t)} = \mathbf{v}^{(1,t)}$ and Eq. (4.3) takes the form*

$$(4.5) \quad X_{tt'} = \tilde{A}_{t,t'} \chi(t) \chi(t').$$

When there is just one layers' centrality matrix that has the largest spectral radius, which one often expects to occur for adjacency matrices and hub/authority matrices (unless the network layers contain symmetries giving rise to repeated spectral radii across layers), then the limiting behavior of the eigenvector is that it localizes onto a single dominating layer.

Corollary 4.5 (Weak-Coupling-Induced Eigenvector Localization onto a Dominating Layer).

Under the assumptions of Thm. 4.2 and assuming that one single layer has a spectral radius that is larger than the other (i.e., $\lambda_{\max} = \mu_1^{(t)}$ for a single layer $t = t^*$), then in the limit as $\omega \rightarrow 0^+$, we have

$$(4.6) \quad \mathbf{v}(\omega) \rightarrow \mathbf{v}^{(1,t^*)}, \quad \mathbf{u}(\omega) \rightarrow \mathbf{u}^{(1,t^*)}.$$

Understanding whether or not the dominant eigenvector localizes onto a single layer, onto several layers (i.e., as given by the function $\chi(t)$), or does not localize has significant practical consequences. In some situations, it can be appropriate to allow eigenvector localization [78], whereas it can be beneficial to avoid localization in other applications [67]. The results presented above characterize localization in the weak-coupling limit and can be used by practitioners to make better-informed choices about which centrality matrices to use.

4.2. Layer Aggregation in the Strong-Coupling Limit. We now study Eq. (3.2) in the limit as $\omega \rightarrow \infty$ (or, equivalently, as $\epsilon = \omega^{-1} \rightarrow 0^+$). The results to follow significantly generalize [102], which assumed that $\tilde{\mathbf{A}}$ encoded adjacent-in-time coupling. We now allow $\tilde{\mathbf{A}}$ to be from a much more general class of matrices, including asymmetric matrices that implement directed interlayer couplings.

Consider the scaled supracentrality matrix

$$(4.7) \quad \tilde{\mathbf{C}}(\epsilon) = \epsilon \mathbf{C}(\epsilon^{-1}) = \epsilon \hat{\mathbf{C}} + \hat{\mathbf{A}},$$

which has eigenvectors $\tilde{\mathbf{u}}(\epsilon)$ and $\tilde{\mathbf{v}}(\epsilon)$ that are identical to those of $\mathbf{C}(\omega)$ (specifically, $\tilde{\mathbf{u}}(\epsilon) = \mathbf{u}(\epsilon^{-1})$ and $\tilde{\mathbf{v}}(\epsilon) = \mathbf{v}(\epsilon^{-1})$); and its eigenvalues $\{\tilde{\lambda}_i\}$ are scaled by ϵ (specifically, $\tilde{\lambda}_i(\epsilon) = \epsilon \lambda_i(\epsilon^{-1})$). To facilitate our presentation, we define a permutation operator for $NT \times NT$ matrices.

Definition 4.6 (Node-Layer-Reordering Stride Permutation). Matrix \mathbb{P} is a T -stride permutation matrix of size $NT \times NT$ if it takes the form [33]

$$(4.8) \quad [\mathbb{P}]_{kl} = \begin{cases} 1, & l = \lceil k/N \rceil + T[(k-1) \bmod N], \\ 0, & \text{otherwise,} \end{cases}$$

so that $(\tilde{\mathbf{A}} \otimes \mathbf{I}) = \mathbb{P}(\mathbf{I} \otimes \tilde{\mathbf{A}})\mathbb{P}^T$.

Remark 4.1. The stride permutation matrix is unitary, and it simply changes the ordering of node-layer pairs. That is, a supracentrality matrix has entries that are ordered first by node i and then by layer t (i.e., $(i, t) = (1, 1), (2, 1), (3, 1), \dots$); after the permutation, the entries are ordered first by layer t and then by node i (i.e., $(i, t) = (1, 1), (1, 2), (1, 3), \dots$). (We note in passing that this permutation is one type of graph isomorphism [54].)

We now present our main findings for the strong-coupling regime.

Theorem 4.7 (Singularity at Infinite Coupling). Assume that the interlayer-adjacency matrix $\tilde{\mathbf{A}}$ is diagonalizable and has T distinct eigenvalues. Let $\{\tilde{\mu}_t\}$ denote its T eigenvalues, and let $\{\tilde{\mathbf{u}}^{(t)}\}$ and $\{\tilde{\mathbf{v}}^{(t)}\}$ denote the corresponding left and right eigenvectors, respectively. We assume that the eigenvalues are simple and are ordered such that $\tilde{\mu}_1$ is the largest eigenvalue. Further, let \mathbb{P} denote the stride permutation matrix given by Eq. (4.8).

For $\epsilon = 0$, the spectrum $\{\tilde{\lambda}_i(0)\}$ of the supracentrality matrix $\mathbb{C}(\epsilon)$ given by Eq. (4.7) is identical to that of $\tilde{\mathbf{A}}$, and each eigenvalue $\tilde{\lambda}_i(0) = \tilde{\mu}_t$ has multiplicity N and an associated N -dimensional left and right eigenspace that is spanned by eigenvectors $\tilde{\mathbf{u}}^{(t)}$ and $\tilde{\mathbf{v}}^{(t)}$, respectively, with the general form

$$(4.9) \quad \tilde{\mathbf{v}}^{(t)} = \sum_j \tilde{\alpha}_{tj} \mathbb{P} \tilde{\mathbf{v}}^{(t,j)}, \quad \tilde{\mathbf{u}}^{(t)} = \sum_j \tilde{\beta}_{tj} \mathbb{P} \tilde{\mathbf{u}}^{(t,j)},$$

where the constants $\{\tilde{\alpha}_{tj}\}$ and $\{\tilde{\beta}_{tj}\}$ must satisfy $\sum_j \tilde{\alpha}_{tj}^2 = \sum_j \tilde{\beta}_{tj}^2 = 1$ to ensure that $\|\tilde{\mathbf{u}}^{(t)}\|_2 = \|\tilde{\mathbf{v}}^{(t)}\|_2 = 1$. The length- NT vectors are given by $\tilde{\mathbf{v}}^{(t,j)} = \tilde{\mathbf{e}}^{(j)} \otimes \mathbf{v}^{(t)}$ and $\tilde{\mathbf{u}}^{(t,j)} = \tilde{\mathbf{e}}^{(j)} \otimes \mathbf{u}^{(t)}$. Here, $\tilde{\mathbf{e}}^{(j)}$ is a length- N unit vector consisting of zeros except for entry j , which is one, so that the vectors $\tilde{\mathbf{u}}^{(t,j)}$ and $\tilde{\mathbf{v}}^{(t,j)}$ consist of zeros except the j -th blocks of size T , which consist of an eigenvector of $\tilde{\mathbf{A}}$.

Proof. See Appendix D. ■

Remark 4.2. It is straightforward to also obtain the general form of eigenvectors for eigenvalues $\{\mu_t\}$ whose multiplicity is more than 1. For example, if the eigenvalue $\tilde{\mu}_t$ of $\tilde{\mathbf{A}}$ has multiplicity q , then $\tilde{\lambda}_i(0) = \tilde{\mu}_t$ has multiplicity qN for matrix $\mathbb{C}(0)$. However, the notation becomes slightly more cumbersome, and we will not study such cases in this paper.

Theorem 4.8 (Strong-Coupling Limit of Dominant Eigenvectors). Let $\tilde{\mu}_1$ denote the dominant eigenvalue (which we assume to be simple) of the interlayer-adjacency matrix $\tilde{\mathbf{A}}$, and let $\tilde{\mathbf{u}}^{(1)}$ and $\tilde{\mathbf{v}}^{(1)}$ denote its left and right eigenvectors. We assume that the constraints of Thm. 3.5 are satisfied, so that the supracentrality matrix $\mathbb{C}(\epsilon)$ given by Eq. (3.1) is nonnegative, irreducible, and aperiodic. It then follows that the dominant eigenvalue $\tilde{\lambda}_{\max}(\epsilon)$ and corresponding eigenvectors $\mathbf{u}^{(1)}(\epsilon)$ and $\mathbf{v}^{(1)}(\epsilon)$ of $\mathbb{C}(\epsilon)$ converge as $\epsilon \rightarrow 0^+$ as follows:

$$(4.10) \quad \tilde{\lambda}_{\max}(\epsilon) \rightarrow \tilde{\mu}_1, \quad \tilde{\mathbf{v}}^{(1)}(\epsilon) \rightarrow \sum_j \tilde{\alpha}_j \mathbb{P} \tilde{\mathbf{v}}^{(1,j)}, \quad \tilde{\mathbf{u}}^{(1)}(\epsilon) \rightarrow \sum_j \tilde{\beta}_j \mathbb{P} \tilde{\mathbf{u}}^{(1,j)},$$

where \mathbb{P} is the stride permutation defined by Eq. (4.8), $\tilde{\mathbf{u}}^{(1,j)}$ and $\tilde{\mathbf{v}}^{(1,j)}$ are defined in Thm. 4.7 and the constants $\{\tilde{\beta}_i\}$ and $\{\tilde{\alpha}_i\}$ solve the dominant eigenvalue equations

$$(4.11) \quad \tilde{\mathbf{X}} \tilde{\boldsymbol{\alpha}} = \tilde{\mu}_1 \tilde{\boldsymbol{\alpha}}, \quad \tilde{\mathbf{X}}^T \tilde{\boldsymbol{\beta}} = \tilde{\mu}_1 \tilde{\boldsymbol{\beta}},$$

where

$$(4.12) \quad \tilde{X}_{ij} = \sum_t C_{ij}^{(t)} \frac{\tilde{u}_t^{(1)} \tilde{v}_t^{(1)}}{\langle \tilde{\mathbf{u}}^{(1)}, \tilde{\mathbf{v}}^{(1)} \rangle}.$$

Proof. See Appendix E. ■

Equation (4.12) indicates that the strong-coupling limit effectively aggregates the centrality matrices $\{\mathbf{C}^{(t)}\}$ across time via a weighted average, with weights that depend on the left and right dominant eigenvectors of the interlayer-adjacency matrix $\tilde{\mathbf{A}}$. This result generalizes Eq. (4.13) in [102], which assumed that $\tilde{\mathbf{A}}$ is symmetric (so that $\tilde{u}_t^{(1)} = \tilde{v}_t^{(1)}$). The result in [102] is recovered with the following.

Corollary 4.9 (Strong-Coupling Limit of Adjacent-in-Time Uniform, Diagonal Coupling [102]).

For adjacent-in-time interlayer coupling, the $\epsilon \rightarrow 0^+$ limit of the largest eigenvalue is $\lambda_1(\epsilon) \rightarrow 2 \cos\left(\frac{\pi}{T+1}\right)$; and the $\epsilon \rightarrow 0^+$ limit of the dominant eigenvector is given by Eqs. (4.10)–(4.12), with

$$\tilde{\mathbf{X}} = \sum_t \mathbf{C}^{(t)} \frac{\sin^2\left(\frac{\pi t}{T+1}\right)}{\sum_{t=1}^T \sin^2\left(\frac{\pi t}{T+1}\right)}.$$

Corollary 4.10 (Strong-Coupling Limit of All-to-All Uniform, Diagonal Coupling). For all-to-all coupling (without self edges), $\tilde{\mathbf{A}} = \mathbf{1}\mathbf{1}^T$, the $\epsilon \rightarrow 0^+$ limit of the largest eigenvalue is $\lambda_{\max}(\epsilon) \rightarrow \tilde{\mu}_1 = N$; and the $\epsilon \rightarrow 0^+$ limit of the dominant eigenvector is given by Eqs. (4.10)–(4.12), with $\tilde{\mathbf{X}} = T^{-1} \sum_t \mathbf{C}^{(t)}$.

Proof. In this case, the largest eigenvalue of $\tilde{\mathbf{A}}$ is $\mu_1 = N$, and the left and right dominant eigenvectors have the same value in each component, with entries $u_t^{(1)} = v_t^{(1)} = T^{-1/2}$. ■

Corollary 4.11 (Strong-Coupling Limit of Rank-1 Uniform, Diagonal Coupling). For a rank-1 coupling matrix, $\tilde{\mathbf{A}} = \tilde{\mathbf{w}}\tilde{\mathbf{w}}^T$, the $\epsilon \rightarrow 0^+$ limit of the largest eigenvalue is $\lambda_{\max}(\epsilon) \rightarrow 1$; and the $\epsilon \rightarrow 0^+$ limit of the dominant eigenvector is given by Eqs. (4.10)–(4.12), with $\tilde{\mathbf{X}} = \sum_t \mathbf{C}^{(t)} \tilde{w}_t^2$.

Proof. This follows from the fact that the largest eigenvalue of $\tilde{\mathbf{A}}$ is $\tilde{\mu}_1 = 1$, with associated eigenvectors $\tilde{u}_t^{(1)} = \tilde{v}_t^{(1)} = \tilde{w}_t$. ■

5. Case Studies with Empirical Data. We now apply the supracentrality framework to study two data sets. In Sec. 5.1, we examine a multiplex network that encodes flight patterns between European airports, with layers representing different airlines companies [13]. In Sec. 5.2, we examine a temporal network that encodes the exchange of mathematicians between mathematical-sciences programs in the United States [102]. These experiments explore different interlayer-coupling strengths and topologies, illustrating strategies for how to flexibly apply the framework to diverse applications.

5.1. European Airport Rankings in a Multiplex Airline Network [13]. We first apply our supracentrality framework to study the importances of European airports using an empirical multiplex network of the flight patterns for $T = 37$ airline companies [13]. See Table SM1 in the Supplementary Material for a list of the airline companies and the number of edges and spectral radii of their associated layers. The network’s nodes represent European airports; we consider only the $N = 417$ nodes in the largest connected component of the network associated with the sum of the layers’ adjacency matrices. We couple the layers using all-to-all coupling ($\tilde{\mathbf{A}} = \mathbf{1}\mathbf{1}^T$) eigenvector centralities with centrality matrices given by Definition 2.3.

For each airport, we compute the joint, marginal, and conditional centralities for a range of coupling strengths ω . In Fig. 4, we plot the MLCs and MNCs (see Definition 3.3). In Fig. 4(a), we see that for large ω , all layers have similar importance; by contrast, for small ω , one layer is much more important due to the eigenvector localization phenomenon that we described in Cor. 4.5. Specifically, the layer that represents Ryanair dominates for small ω , as its adjacency matrix has the largest spectral radius. (It also has the largest number of edges.) Previous investigation of multilayer centralities in this data set [84] also identified Ryanair as the most important layer.

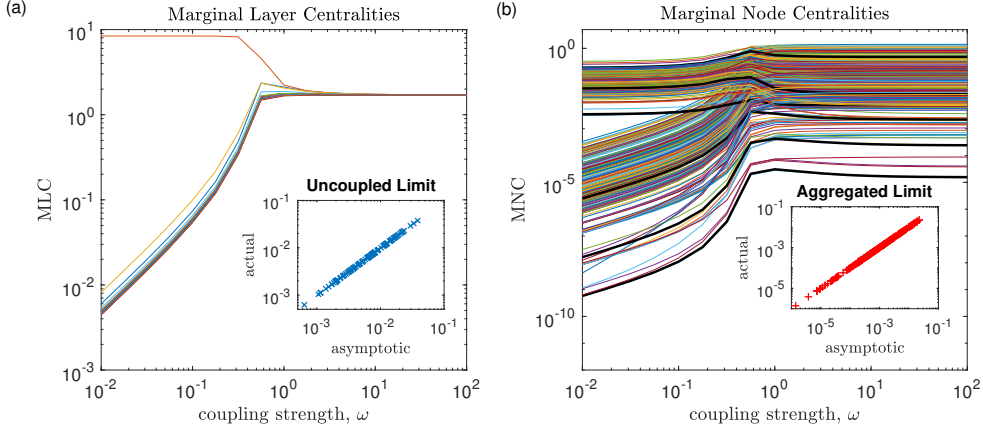


Figure 4. MLCs and MNCs for a multiplex European airline transportation network of flight patterns for 37 airlines [13]. We couple the layers with all-to-all coupling and examine $\omega \in [10^{-2}, 10^2]$. The insets in (a) and (b) compare observed conditional node centralities for $\omega = 10^{-2}$ and $\omega = 10^2$, respectively, to the asymptotic values from Thms. 4.2 and 4.8.

The insets in Fig. 4 give the conditional centralities of nodes for $\omega = 10^{-2}$ (in panel (a)) and $\omega = 10^2$ (in panel (b)) versus the asymptotic values in the associated limits $\omega \rightarrow 0^+$ (see Thm. 4.2) and $\omega \rightarrow \infty$ (see Thm. 4.8), demonstrating that they are in excellent agreement. One can also observe in Fig. 4(b) that there is not a simple transition between these two limits. Specifically, the thick black curves highlight a few airports whose centralities have a peak for intermediate values of ω . That is, these airports are more important if one considers the airline network as a multiplex network, whereas they are less important if one considers the layers in isolation or in aggregate.

Table 2

European airports with the highest MNCs for three coupling strengths ω that correspond to the regimes of weak, intermediate, and strong coupling. These computations are of eigenvector centralities with all-to-all, uniform and diagonal coupling between layers. We indicate airports with their International Civil Aviation Organization (ICAO) code.

Rank	$\omega = 0.01$		$\omega = 1$		$\omega = 100$	
	Airport	MNC	Airport	MNC	Airport	MNC
1	EGSS	0.329	LEMD	1.379	EHAM	1.406
2	EIDW	0.286	EHAM	1.296	LEMD	1.400
3	LIME	0.254	LEBL	1.257	LIRF	1.206
4	EBCI	0.201	EDDM	1.171	LOWW	1.198
5	LEMD	0.193	LIRF	1.150	LEBL	1.193
6	LEAL	0.190	EDDF	1.121	EDDM	1.160
7	EDFH	0.189	EDDL	1.105	LFPG	1.157
8	LIRA	0.184	LFPG	1.091	EDDF	1.134
9	LEGE	0.176	LOWW	1.066	EDDL	1.128
10	LEPA	0.166	LIMC	0.968	LSZH	1.017

In Table 2, we list the airports with the highest MLCs for small, intermediate, and large

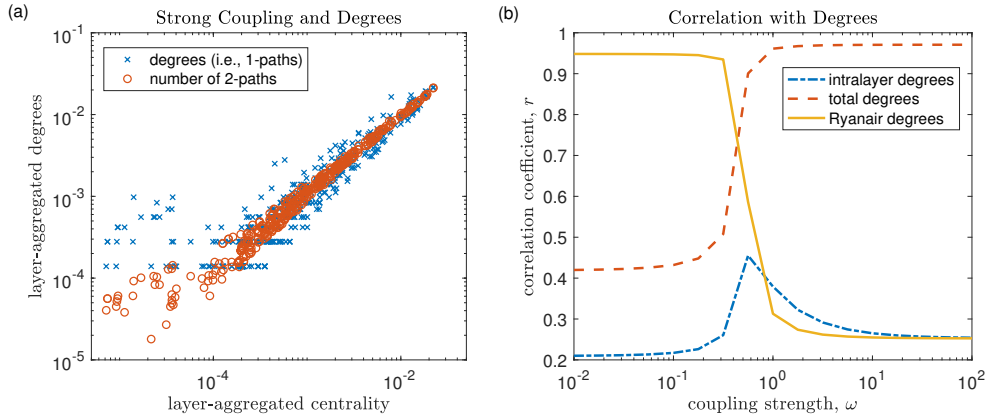


Figure 5. Eigenvector supracentralities for the multiplex European airline network. (a) For $\omega = 100$, the airports’ marginal-node centralities correlate strongly with the layer-aggregated degrees, $d_i = \sum_{t,j} A_{ij}^{(t)}$, and with the total number of length-2 paths (summed across layers) emanating from each node, $\sum_{t,j} [A_{ij}^{(t)}]^2$. (To facilitate this comparison, we encode values in normalized vectors.) (b) Pearson correlation coefficients for comparing the airports’ supracentralities to different types of node degree for multiplex networks (see text).

values of ω for eigenvector supracentrality. As expected, for large and small ω , the top airports correspond to the top (i.e., highest eigenvector centrality) airports associated with the aggregation of layers and the Ryanair network layer, respectively. The top-ranked airports for $\omega = 1$ have a large overlap with those for $\omega = 100$; however, the top airport, Adolfo Suárez Madrid–Barajas Airport (LEMD), is particularly interesting. LEMD is the only airport that ranks in the top 10 for both the Ryanair network layer and the layer-aggregated network; this contributes to its having the highest rank for this moderate value of ω . We highlight similar ranking boosts for other airports by solid black curves in Fig. 4(b). We also note that LEMD was identified in previous investigations [47, 107] as one of the most important airports in this data set.

In Fig. 5, we show that the eigenvector supracentralities correlate strongly with node degrees. In Fig. 5(a), we show for $\omega = 100$ that the airports’ conditional centralities, averaged across layers, are correlated strongly with their total (i.e., layer-aggregated) degrees $\bar{d}_i = \sum_{t,j} A_{ij}^{(t)}$ (see the blue ‘x’ marks). This strong correlation is expected for eigenvector centrality, as the degrees are a first-order approximation to eigenvector centrality [103]. We also plot the mean conditional centralities versus the number of length-2 paths that emanate from each node (see the red circles). As expected, they exhibit an even stronger correlation, as the number of length-2 paths provides a second-order approximation to eigenvector centrality [103]³.

³As described in [103], one can interpret the number of length- k paths as an order- k approximation to the dominant eigenvector of a matrix by considering the power-method iteration for numerically computing the dominant eigenvector. If one initializes the power method with a vector of ones, $\mathbf{1}$, then $\mathbf{B}^k \mathbf{1}$ converges (after normalization) to the dominant eigenvector of matrix \mathbf{B} (which additionally assumes the dominant eigenspace is 1 dimensional). If the matrix happens to be an adjacency matrix, $\mathbf{B} = \mathbf{A}$, then $[\mathbf{A}^k \mathbf{1}]_i$ also happens to be the number of length- k paths emanating from node i .

In Fig. 5(b), we plot (as a function of ω) the Pearson correlation coefficient r between node degrees and eigenvector centralities for three cases: total degrees $\{\bar{d}_i\}$ and marginal node centralities; intralayer degrees $\{d_i^{(t)} = \sum_j A_{ij}^{(t)}\}$ and conditional centralities; and degrees in the Ryanair layer $\{d_i^{(2)} = \sum_j A_{ij}^{(2)}\}$ and marginal node centralities. As expected for very small and large values of ω , the supracentralities correlate strongly with the Ryanair layer and the layer-aggregated network, respectively. Interestingly, for moderate values of ω , there is a spike in the correlation between conditional node centralities and the intralayer degrees $\{d_i^{(t)}\}$.

In Sec. SM2 of the Supplementary Material, we describe results repeating this experiment with PageRank matrices (see Definition 2.5). Fig. SM2 provides an interesting contrast to Fig. 5(b). Because PageRank matrices have the same spectral radius, no layer dominates in the limit of small ω , so there is no eigenvector localization (see Thm. 4.2). Instead, in Fig. SM2(b) we observe for small ω that the conditional centralities correlate strongly with the nodes' intralayer degrees $\{d_i^{(t)}\}$.

5.2. United States Mathematical-Science Program Rankings using a Ph.D. Exchange Network. We apply our supracentrality framework to study the prestige of U.S. mathematics programs by examining a temporal network that encodes the graduation and hiring of Ph.D.s in the mathematical sciences [102]. The data set was constructed using the Mathematics Genealogy Project [82]. As in [102], we calculate uniformly and diagonally coupled authority scores so that universities with a high authority score correspond to academic authorities. They produce desirable students to be hired by other institutions. In [102], we restricted our attention to undirected, adjacent-in-time coupling encoded by an interlayer adjacency matrix $\tilde{\mathbf{A}}$ with entries $\tilde{A}_{tt'} = 1$ if $|t - t'| = 1$ and $\tilde{A}_{tt'} = 0$ otherwise. In the current study, by contrast, we consider the effects of causality by coupling time layers using a directed chain with “teleportation” encoded by the interlayer adjacency matrix

$$(5.1) \quad \tilde{A}_{tt'} = \begin{cases} 1, & t' - t = 1, \\ \gamma, & \text{otherwise.} \end{cases}$$

Teleportation was introduced for PageRank centrality [32] to allow the centrality matrices associated with weakly-connected (and even disconnected) networks to satisfy the irreducibility assumptions of Theorems 2.6 and 2.7. Similarly, we use teleportation between layers to satisfy the assumptions of Thm. 3.5, which ensures that the supracentralities are positive and unique. We differentiate these two types of teleportation by referring to the original PageRank notion as *node teleportation* and the teleportation in Eq. 5.1 as *layer teleportation*.

In Fig. 6, we examine the effect of the layer-teleportation parameter γ on supracentralities. In Fig. 6(a)–(c), we plot the layers' authority MLCs $x_t(\omega)$ given by Definition 3.3 versus the year t for three coupling strengths, $\omega \in \{10^1, 10^2, 10^3\}$, which correspond to the weak, intermediate, and strong-coupling regimes. In each panel, we plot the MLC for three values of the teleportation parameter: $\gamma = 10^{-2}$, $\gamma = 10^{-3}$, and $\gamma = 10^{-4}$. In panel (d), we plot $\bar{d}_t = \sum_{ij} A_{ij}^{(t)}$, which is the total number of graduating mathematical-sciences Ph.D.s in year t who later supervised a graduating Ph.D. student. Observe that $t = 1966$ is the year in which \bar{d}_t is the largest.

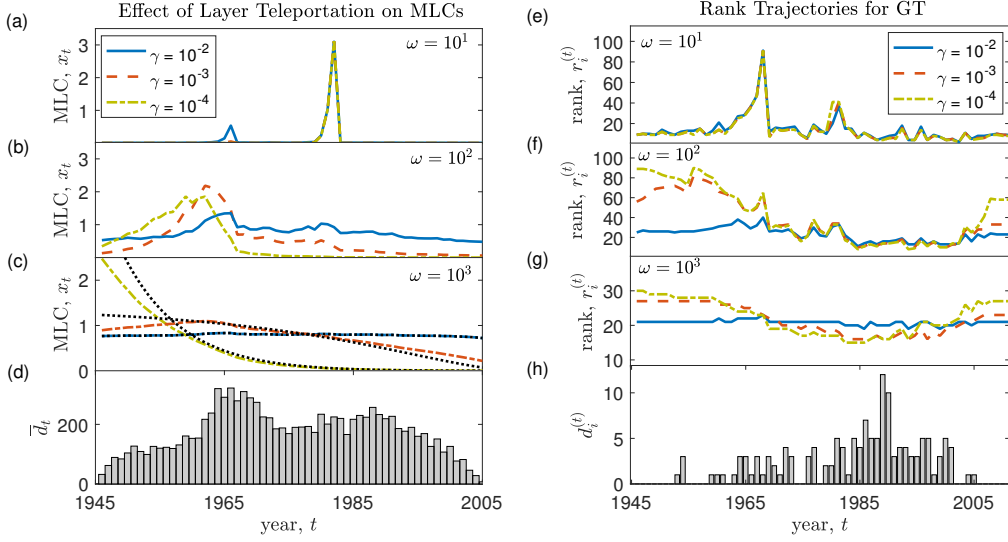


Figure 6. Effect of layer teleportation parameter γ on authority supracentralities in the mathematical-sciences Ph.D. exchange network [102]. (a)–(c) MLC versus year t for several choices of γ and ω . The black dotted curves in (c) depict the asymptotic results from the $\omega \rightarrow \infty$ limit given by Thm. 4.8 (in this case, the dominant right eigenvector of $\tilde{\mathbf{A}}$). (d) The total number of graduating mathematical-sciences Ph.D.s in year t who later supervised a graduating Ph.D. student, $\bar{d}_t = \sum_{ij} A_{ij}^{(t)}$. (e)–(g) Rank $r_i^{(t)}$ associated with conditional centrality for Georgia Institute of Technology (GT) for various values of γ and ω . (h) The number $\bar{d}_i^{(t)} = \sum_j A_{ij}^{(t)}$ of mathematical-sciences Ph.D.s who graduated at GT in year t who later supervised a graduating student.

In Fig. 6(a), i.e., for small ω , we observe eigenvector localization onto time layer $t = 1982$, whose associated authority matrix has the largest spectral radius among all layers. For $\gamma = 10^{-2}$, we also observe a smaller peak at $t = 1966$, which arises for moderate values of γ and ω but ultimately vanishes as $\omega \rightarrow 0^+$. Comparing panel (b) to panel (a) for $\gamma = 10^{-2}$, the peak near $t = 1966$ is more pronounced for $\omega = 10^1$ than for $\omega = 10^2$. We observed a similar localization phenomena in [102] for adjacent-in-time coupling. By contrast, Fig. 6(c) illustrates behavior that is very different from findings in [102]. We see that the interlayer-adjacency matrix (which changes with the teleportation parameter γ) is very important for the strong-coupling limit. By varying γ , one can tune the extent to which older time layers have higher centrality than newer time layers. When $\gamma = 10^{-4}$, for example, one can observe in Fig. 6(c) that the MLC of time layers appears to rapidly drop off as t increases. This phenomenon is accurately described by our asymptotic theory in Sec. 4.2 — the dotted black curves show the right dominant eigenvector vector $\tilde{\mathbf{v}}^{(1)}$ of $\tilde{\mathbf{A}}$ (after normalization), which we obtain from Thm. 4.8 as the asymptotic $\omega \rightarrow \infty$ limit for MLC.

In Fig. 6(e)–(g), we plot the university rank $r_i^{(t)} \in \{1, \dots, N\}$ of Georgia Institute of Technology (GT) associated with the university’s conditional centralities for different time layers. Similar to panels (a)–(c), these panels depict results for $\omega \in \{10, 10^2, 10^3\}$; in each panel, we again plot results for $\gamma \in \{10^{-2}, 10^{-3}, 10^{-4}\}$. In Fig. 6(h), we plot the number of graduating mathematical-science Ph.D.s from GT who later supervise a graduating Ph.D. student, observing that this increases starting in the 1960s. We used GT in [102] as a case

study to illustrate the methods developed there. In the current case study, we highlight that the choices for ω and γ influence the centrality trajectory for GT. Note that γ has a larger effect for the intermediate- and strong-coupling regimes (see panels (f) and (g)) than for the weak-coupling regime. Observe for moderate values of γ and ω that GT has a rank trajectory in which its rank varies from about 50th to about 15th during the period $t \in [1945, 1985]$. In Section SM3 of the Supplementary Materials, we show that although γ has a strong effect on the MLCs for large ω , it does not seem to have a significant effect on top-ranking schools. In Fig. SM3 of the Supplementary Materials, we show that — similar to the results in Fig. 5(b) — for the limit of small and large ω , the supracentralities correlate with the intralayer degrees of a dominating layer ($t = 1966$ in this case) and with the nodes’ total degrees, respectively. We finally highlight that all centrality trajectories for GT presented here significantly differ from those presented in [102], which implemented coupled time layers using an undirected chain. In particular, many of the rank trajectories in Fig. 6(e)–(g) show GT having its highest rank in the 1980s, around the time when GT graduated its largest numbers of future-adviser Ph.D. students.

6. Conclusions. It is important to develop systematic ways of calculating importances in the form of centrality and its generalizations for nodes, edges, and other structures in multilayer networks. In this paper, we examined centralities based on eigenvectors for two popular classes of multilayer networks: multiplex networks that encode different types of relationships, and temporal networks in which the relationships change in time. We presented a unifying linear-algebraic framework that generalizes eigenvector-based centralities, such as PageRank and hub/authority scores, for multiplex and temporal networks. A key aspect of our approach involves studying joint, marginal, and conditional centralities that one obtains from the dominant eigenvector of a supracentrality matrix, which couples centrality matrices associated with individual layers.

Our main methodological contribution is the extension of the supracentrality framework [102], which was previously restricted to adjacent-in-time coupling. Our new, more general framework couples layers through an interlayer adjacency matrix $\tilde{\mathbf{A}}$, allowing for a large family of interlayer coupling topologies. (See Thm. 3.5 for assumptions that ensure the supracentralities to be well behaved.) We find $\tilde{\mathbf{A}}$ to significantly impact supracentralities, and some choices are more appropriate than others for different applications. As an example, in Sec. 5.2 we let $\tilde{\mathbf{A}}$ encode a directed chain with layer teleportation (see Fig. 1(b) for visualization) and study a temporal network encoding the graduation and hiring of mathematics Ph.D.s. Our results significantly contrast with those in [102] due to our different choice of interlayer coupling. We found coupling using a directed chain (which respects the arrow of time) to introduce a bias that increases the centralities of node-layer pairs associated with the earliest time layers. This bias can be moderated by the layer teleportation parameter. We also studied a multiplex network representing airline transportation in Europe (Sec. 5.1), where another mechanism gives rise to boosts in centrality. See [99] for MATLAB code that computes supracentralities and reproduces the experimental results presented in this paper.

We identify an interesting interplay between the topology of the interlayer coupling $\tilde{\mathbf{A}}$ and the topologies of the individual layers in multiplex/temporal networks. We gained insight by developing singular perturbation theory for the limits of weak and strong interlayer coupling

(Sec. 4), which respectively lead to layer decoupling and layer aggregation. We found the limiting supracentralities to depend on several factors including the dominant left and right eigenvectors of $\tilde{\mathbf{A}}$ as well as the spectral radii of the layers' centrality matrices, possibly leading to a phenomenon in which the dominant eigenvector localizes onto one or more layers (particularly, the layers with centrality matrices having the largest spectral radii). We expect these results to be broadly insightful for the study of "supramatrices" in general, and possible other situations that may benefit from coupling together the dominant eigenvectors of several matrices.

Appendix A. Proof of Theorem 3.5. The uniqueness and positivity of $\mathbf{v}(\omega)$ are guaranteed by Perron–Frobenius theory [4] (see Thm. 2.6). We assume that $\tilde{\mathbf{A}}$ is nonnegative and irreducible and that the summation $\sum_t \mathbf{C}^{(t)}$ is an irreducible nonnegative matrix. It remains to show that these assumptions imply that $\mathbb{C}(\omega)$ is irreducible and nonnegative. Note that the entries in $\mathbb{C}(\omega)$ are nonnegative, and we can interpret it as a weighted adjacency matrix for node-layer pairs $\{(i, t)\}$. In particular, under the above assumptions, $\mathbb{C}(\omega)$ corresponds to an adjacency matrix of a strongly-connected graph. This follows from two observations: First, because $\tilde{\mathbf{A}}$ describes an adjacency matrix for a strongly connected graph, any node-layer pair (i, t) is connected to all other node-layer pairs $\{(i, t)\}$ that involve the same node i . Second, because $\overline{\mathbf{C}^{(t)}} = T^{-1} \sum_t \mathbf{C}^{(t)}$ is irreducible and nonnegative, it follows that for any pair of nodes $(i, j) \in \mathcal{V} \times \mathcal{V}$ in layer t , there exists a value k such that $[\overline{\mathbf{C}^{(t)}}]^{k'} > 0$, and there is thus a path between this pair in the network associated with $\overline{\mathbf{C}^{(t)}}$.

Because $\mathbb{C}(\omega)$ corresponds to a strongly-connected graph, it is irreducible and nonnegative, so $\mathbf{v}(\omega)$ is unique and positive. It follows that the entries $\{W_{it}(\omega)\}$, $\{x_i(\omega)\}$, and $\{\hat{x}_t(\omega)\}$ are also positive and unique. Because these entries are positive, it is also the case that $\{Z_{it}(\omega)\}$ and $\{\hat{Z}_{it}(\omega)\}$ are positive and finite-valued.

If $\mathbb{C}(\omega)$ is aperiodic, then Thm. 2.6 states that the largest positive eigenvalue is the unique dominant eigenvalue.

Appendix B. Proof of Theorem 4.1. For any choice of matrix norm, $\|\mathbb{C}(\omega) - \hat{\mathbb{C}}\| = \omega \|\hat{\mathbf{A}}\| \rightarrow 0^+$ as $\omega \rightarrow 0^+$ (recall that $\hat{\mathbf{A}} = \tilde{\mathbf{A}} \otimes \mathbf{I}$), implying that

$$(B.1) \quad \mathbb{C}(\omega) \rightarrow \hat{\mathbb{C}} = \text{diag} \left[\mathbf{C}^{(1)}, \mathbf{C}^{(2)}, \dots, \mathbf{C}^{(T)} \right].$$

We assume that the eigenvalues $\{\mu_i^{(t)}\}$ of each $\mathbf{C}^{(t)}$ are simple and that $\{\mu_i^{(t)}\} \cap \{\mu_i^{(t')}\} = \emptyset$ when $t \neq t'$. Considering the matrix-vector multiplication $\hat{\mathbb{C}} \mathbf{v}^{(i,t)}$, we use $k = s \bmod(N)$ and $t' = \lceil s/jN \rceil$ to obtain

$$(B.2) \quad [\hat{\mathbb{C}} \mathbf{v}^{(i,t)}]_s = \sum_{(k,t')} C_{jk}^{(t)} v_k^{(i,t')} \delta_{tt'} = \mu_i^{(t)} v_j^{(i,t')} \delta_{tt'} = \mu_i^{(t)} [\mathbf{v}^{(i,t)}]_s.$$

This implies that $\hat{\mathbb{C}} \mathbf{v}^{(i,t)} = \mu_i^{(t)} \mathbf{v}^{(i,t)}$, so $\mu_i^{(t)}$ is an eigenvalue of $\hat{\mathbb{C}}$ with right eigenvector $\mathbf{v}^{(i,t)}$. Similarly, $\hat{\mathbb{C}}^T \mathbf{u}^{(i,t)} = \mu_i^{(t)} \mathbf{u}^{(i,t)}$, so $\mathbf{u}^{(i,t)}$ is the associated left eigenvector.

We now show that when the eigenvalue $\mu_i^{(t)}$ is not simple, such that $\mu_i^{(t)} = \lambda_n(0)$ for some set $\mathcal{P} = \{(i, t)\}$ with cardinality $P = |\mathcal{P}| > 1$, it has P -dimensional left and right eigenspaces

that are spanned by the associated left and right eigenvectors $\{\mathbf{u}^{(i,t)}\}$ and $\{\mathbf{v}^{(i,t)}\}$. To see this, let $\tilde{\mathbf{u}} = \sum_{(i,t)} \beta_{i,t} \mathbf{u}^{(i,t)}$ and $\tilde{\mathbf{v}} = \sum_{(i,t)} \alpha_{i,t} \mathbf{v}^{(i,t)}$ denote any linear combination of such vectors, and consider the matrix-vector multiplication

$$\begin{aligned}
[\hat{\mathbb{C}}\tilde{\mathbf{v}}]_s &= \sum_{(k,t')} C_{jk}^{(t)} \sum_{(i,t) \in \mathcal{P}} \alpha_{i,t} v_k^{(i,t')} \delta_{tt'} \\
&= \sum_{(i,t) \in \mathcal{P}} \alpha_{i,t} \mu_i^{(t)} v_j^{(i,t)} \delta_{tt'} \\
&= \lambda_n \sum_{(i,t) \in \mathcal{P}} \alpha_{i,t} v_j^{(i,t)} \delta_{tt'} \\
\text{(B.3)} \qquad &= \lambda_n [\tilde{\mathbf{v}}]_s,
\end{aligned}$$

so that $\hat{\mathbb{C}}\tilde{\mathbf{v}} = \lambda_n \tilde{\mathbf{v}}$. One shows similarly that $\hat{\mathbb{C}}^T \tilde{\mathbf{u}} = \lambda_n \tilde{\mathbf{u}}$, which completes the proof.

Appendix C. Proof of Theorem 4.2. Equation (4.1) follows directly from Thm. 4.1, so the $\omega \rightarrow 0^+$ limiting dominant eigenvalue $\lambda_{\max}(0)$ has a P -dimensional dominant eigenspace that is spanned by the left and right eigenvectors, $\{\mathbf{u}^{(i,t)}\}$ and $\{\mathbf{v}^{(i,t)}\}$, associated with $\mathcal{P} = \{(i,t) : \mu_i^{(t)} = \lambda_{\max}(0)\}$. We still need to prove that the constants $\{\alpha_p\}$ and $\{\beta_p\}$ satisfy Eqs. (4.2).

We expand $\lambda_{\max}(\omega)$, $\mathbf{u}^{(1)}(\omega)$, and $\mathbf{v}^{(1)}(\omega)$ for small ω to obtain order- k approximations:

$$\begin{aligned}
\lambda_{\max}(\omega) &= \sum_{j=0}^k \omega^j \lambda_j + \mathcal{O}(\omega^{k+1}), \\
\mathbf{v}^{(1)}(\omega) &= \sum_{j=0}^k \omega^j \mathbf{v}_j + \mathcal{O}(\omega^{k+1}), \\
\text{(C.1)} \qquad \mathbf{u}^{(1)}(\omega) &= \sum_{j=0}^k \omega^j \mathbf{u}_j + \mathcal{O}(\omega^{k+1}).
\end{aligned}$$

We use superscripts to indicate powers of ω in the terms in the expansion, and we use subscripts for the terms that are multiplied by the power of ω . Note that λ_0 , \mathbf{u}_0 , and \mathbf{v}_0 , respectively, indicate the dominant eigenvalue and its corresponding left and right eigenvectors in the limit $\omega \rightarrow 0^+$. Successive terms in these expansions represent higher-order derivatives, and each term assumes appropriate smoothness of these functions. Our strategy is to develop consistent solutions to $\mathbb{C}(\omega)^T \mathbf{u}^{(1)}(\omega) = \lambda_{\max}(\omega) \mathbf{u}^{(1)}(\omega)$ and $\mathbb{C}(\omega) \mathbf{v}^{(1)}(\omega) = \lambda_{\max}(\omega) \mathbf{v}^{(1)}(\omega)$ for progressively larger values of k . Starting with the first-order approximation, we insert $\lambda_{\max}(\omega) \approx \lambda_0 + \omega \lambda_1$ and $\mathbf{v}^{(1)}(\omega) \approx \mathbf{v}_0 + \omega \mathbf{v}_1$ into Eq. (3.2) and collect the zeroth-order and first-order terms in ω to obtain

$$\text{(C.2)} \qquad (\lambda_0 \mathbb{I} - \hat{\mathbb{C}}) \mathbf{v}_0 = 0,$$

$$\text{(C.3)} \qquad (\lambda_0 \mathbb{I} - \hat{\mathbb{C}}) \mathbf{v}_1 = (\hat{\mathbb{A}} - \lambda_1 \mathbb{I}) \mathbf{v}_0,$$

where \mathbb{I} is the $NT \times NT$ identity matrix. Equation (C.2) corresponds to the system described by Thm. 4.1, implying that the operator $\lambda_0 \mathbb{I} - \hat{\mathbf{C}}$ is singular and has a K -dimensional null space, where $K = |\{t : \mu_t = \max_t \mu_t\}|$ is the number of centrality matrices $\mathbf{C}^{(t)}$ whose largest eigenvalue is equal to the maximum eigenvalue. In particular, $\max_t \mu_t = \lambda_0 = \lambda_{\max}(0)$, and the dominant eigenvectors have the general form

$$(C.4) \quad \mathbf{v}_0 = \sum_t \alpha_t \mathbf{v}^{(1,t)}, \quad \mathbf{u}_0 = \sum_t \beta_t \mathbf{u}^{(1,t)},$$

where $\{\alpha_t\}$ and $\{\beta_t\}$ are constants that satisfy $1 = \sum_t \alpha_t^2 = \sum_t \beta_t^2$ to ensure that $\|\boldsymbol{\alpha}\| = \|\boldsymbol{\beta}\| = 1$. (See Thm. 4.1 for definitions of $\mathbf{u}^{(1,t)}$ and $\mathbf{v}^{(1,t)}$.)

To determine the vectors $\boldsymbol{\alpha} = [\alpha_1, \dots, \alpha_T]^T$ and $\boldsymbol{\beta} = [\beta_1, \dots, \beta_T]^T$ of constants that uniquely determine \mathbf{u}_0 and \mathbf{v}_0 , we seek a solvability condition in the first-order terms using Eq. (C.3). We use the fact that the left null space of $\lambda_0 \mathbb{I} - \hat{\mathbf{C}}$ is the span of $\{\mathbf{u}^{(1,t)}\}$ to see that $[\mathbf{u}^{(1,t)}]^T (\lambda_0 \mathbb{I} - \hat{\mathbf{C}}) \mathbf{v}_1 = 0$ for any t . We therefore left-multiply Eq. (C.3) by $[\mathbf{u}^{(1,t)}]^T$ and simplify to obtain

$$(C.5) \quad [\mathbf{u}^{(1,t)}]^T \hat{\mathbf{A}} \mathbf{v}_0 = \lambda_1 [\mathbf{u}^{(1,t)}]^T \mathbf{v}_0.$$

Using the solution of \mathbf{v}_0 given by Eq. (C.4), we obtain

$$(C.6) \quad \begin{aligned} \sum_{t'} \alpha_{t'} [\mathbf{u}^{(1,t)}]^T \hat{\mathbf{A}} \mathbf{v}^{(1,t')} &= \lambda_1 \sum_{t'} \alpha_{t'} [\mathbf{u}^{(1,t)}]^T \mathbf{v}^{(1,t')} \\ &= \lambda_1 \langle \mathbf{u}^{(1,t)}, \mathbf{v}^{(1,t)} \rangle \alpha_t, \end{aligned}$$

which uses $[\mathbf{u}^{(1,t)}]^T \mathbf{v}^{(1,t)} = \langle \mathbf{u}^{(1,t)}, \mathbf{v}^{(1,t)} \rangle \delta_{tt'}$, where δ_{ij} is the Kronecker delta. We simplify the left-hand-side of Eq. (C.6) to obtain

$$(C.7) \quad \begin{aligned} \sum_{t'} \alpha_{t'} [\mathbf{u}^{(1,t)}]^T \hat{\mathbf{A}} \mathbf{v}^{(1,t')} &= \sum_{t'} \alpha_{t'} A_{t,t'} [\mathbf{u}^{(1,t)}]^T [\mathbf{e}^{(t')} \otimes \mathbf{v}^{(1,t')}] \\ &= \sum_{t'} \alpha_{t'} A_{t,t'} [\mathbf{e}^{(t)} \otimes \mathbf{u}^{(1,t)}]^T [\mathbf{e}^{(t')} \otimes \mathbf{v}^{(1,t')}] \\ &= \sum_{t'} \alpha_{t'} A_{t,t'} \langle \mathbf{u}^{(1,t)}, \mathbf{v}^{(1,t')} \rangle. \end{aligned}$$

The last expression follows from the relations $\hat{\mathbf{A}} = \tilde{\mathbf{A}} \otimes \mathbf{I}$, $\mathbf{v}^{(1,t')} = \mathbf{e}^{(t')} \otimes \mathbf{v}^{(1,t')}$, and $\mathbf{u}^{(1,t)} = \mathbf{e}^{(t)} \otimes \mathbf{u}^{(1,t)}$, where we recall that $\mathbf{e}^{(t)}$ is a unit vector consisting of zeros except for entry t , which is one. We set Eq. (C.7) equal to Eq. (C.6) and divide by $\langle \mathbf{u}^{(1,t)}, \mathbf{v}^{(1,t)} \rangle$ to obtain the dominant right eigenvalue equation

$$(C.8) \quad \sum_{t'} A_{t,t'} \frac{\langle \mathbf{u}^{(1,t)}, \mathbf{v}^{(1,t')} \rangle}{\langle \mathbf{u}^{(1,t)}, \mathbf{v}^{(1,t)} \rangle} \alpha_{t'} = \lambda_1 \alpha_t.$$

One proceeds analogously to obtain the left dominant eigenvector equations, and together these two eigenvector equations yield Eq. (4.2).

Appendix D. Proof of Theorem 4.7. Examining $\tilde{\mathbf{C}}(\epsilon)$, which is given by Eq. (4.7), yields (using any matrix norm) $\|\tilde{\mathbf{C}}(\epsilon) - \hat{\mathbf{A}}\| = \epsilon \|\hat{\mathbf{C}}\| \rightarrow 0^+$ as $\epsilon \rightarrow 0^+$, implying that $\tilde{\mathbf{C}}(0) = \hat{\mathbf{A}} = \tilde{\mathbf{A}} \otimes \mathbf{I}$. Using the stride permutation \mathbb{P} defined by Eq. (4.8), we can write

$$(D.1) \quad \mathbb{P}^T(\tilde{\mathbf{A}} \otimes \mathbf{I})\mathbb{P} = \mathbf{I} \otimes \tilde{\mathbf{A}} = \begin{bmatrix} \tilde{\mathbf{A}} & 0 & \cdots \\ 0 & \tilde{\mathbf{A}} & \ddots \\ \vdots & \ddots & \ddots \end{bmatrix}.$$

Because $\mathbf{I} \otimes \tilde{\mathbf{A}}$ is block diagonal, and each diagonal block is identical, the spectrum of $\mathbf{I} \otimes \tilde{\mathbf{A}}$ is identical to that of $\tilde{\mathbf{A}}$ (although the eigenvalues repeat an appropriate number of times), and one can obtain the eigenvectors of the former as functions of the eigenvectors of $\tilde{\mathbf{A}}$, which we assume to be diagonalizable. Let $\{\tilde{\mu}_t\}$ denote the eigenvalues of $\tilde{\mathbf{A}}$, and let $\tilde{\mathbf{u}}^{(t)}$ and $\tilde{\mathbf{v}}^{(t)}$ denote the corresponding left and right eigenvectors, respectively. We now illustrate that $\tilde{\mathbf{u}}^{(t,j)} = \tilde{\mathbf{e}}^{(j)} \otimes \mathbf{u}^{(t)}$ and $\tilde{\mathbf{v}}^{(t,j)} = \tilde{\mathbf{e}}^{(j)} \otimes \mathbf{v}^{(t)}$ are left and right eigenvectors of $\mathbf{I} \otimes \tilde{\mathbf{A}}$. With $s \in \{1, \dots, TN\}$, we define $t = s \bmod(T)$ and $k = \lceil t/sT \rceil$ and obtain

$$(D.2) \quad \begin{aligned} [(\mathbf{I} \otimes \tilde{\mathbf{A}})\hat{\mathbf{v}}^{(t,j)}]_s &= \sum_{t',k'} \tilde{A}_{tt'} \delta_{kk'} \tilde{v}_{t'}^{(t)} \delta_{k'j} \\ &= \sum_{t',k'} \tilde{A}_{tt'} \tilde{v}_{t'}^{(t)} \delta_{kj} \\ &= \sum_{t'} \tilde{A}_{tt'} \tilde{v}_{t'}^{(t)} \delta_{kj} \\ &= \tilde{\mu}_t \tilde{v}_{t'}^{(t)} \delta_{kj} \\ &= \tilde{\mu}_t [\hat{\mathbf{v}}^{(t,j)}]_s. \end{aligned}$$

One can show similarly that $(\mathbf{I} \otimes \tilde{\mathbf{A}})^T \tilde{\mathbf{u}}^{(t,j)} = \tilde{\mu}_t \tilde{\mathbf{u}}^{(t,j)}$, illustrating that $\tilde{\mathbf{u}}^{(t,j)}$ and $\tilde{\mathbf{v}}^{(t,j)}$ are left and right eigenvectors associated to each eigenvalue $\tilde{\mu}_t$ of $\mathbf{I} \otimes \tilde{\mathbf{A}}$. This implies that $\mathbb{P}^T(\tilde{\mathbf{A}} \otimes \mathbf{I})\mathbb{P}\tilde{\mathbf{v}}^{(t,j)} = \mu_t \tilde{\mathbf{v}}^{(t,j)}$, and left-multiplication by \mathbb{P} gives

$$(D.3) \quad (\tilde{\mathbf{A}} \otimes \mathbf{I})[\mathbb{P}\tilde{\mathbf{v}}^{(t,j)}] = \tilde{\mu}_t [\mathbb{P}\tilde{\mathbf{v}}^{(t,j)}].$$

Similarly, one can also show that $(\tilde{\mathbf{A}} \otimes \mathbf{I})^T [\mathbb{P}\tilde{\mathbf{u}}^{(t,j)}] = \tilde{\mu}_t [\mathbb{P}\tilde{\mathbf{u}}^{(t,j)}]$, implying that $\mathbb{P}\tilde{\mathbf{u}}^{(t,j)}$ and $\mathbb{P}\tilde{\mathbf{v}}^{(t,j)}$ are left and right eigenvectors of $\hat{\mathbf{A}} = \tilde{\mathbf{A}} \otimes \mathbf{I}$ associated with the eigenvalue $\tilde{\mu}_t$. However, for a given value of t (and assuming that the eigenvalues $\{\tilde{\mu}_t\}$ are simple), there are N orthogonal left and right eigenvectors $\{\mathbb{P}\tilde{\mathbf{u}}^{(t,j)}\}$ and $\{\mathbb{P}\tilde{\mathbf{v}}^{(t,j)}\}$, respectively, for $j \in \{1, \dots, N\}$. It follows that each eigenvalue $\tilde{\mu}_t$ of $\tilde{\mathbf{A}}$ has multiplicity N , is associated with N eigenvectors, and the general form for an eigenvector is a linear combination of these N eigenvectors.

Appendix E. Proof of Theorem 4.8. We expand $\tilde{\lambda}_{\max}(\epsilon)$, $\tilde{\mathbf{v}}^{(1)}(\epsilon)$, and $\tilde{\mathbf{u}}^{(1)}(\epsilon)$ for small

ϵ to obtain order- k approximations:

$$(E.1) \quad \begin{aligned} \tilde{\lambda}_{\max}(\epsilon) &= \sum_{j=0}^k \epsilon^j \tilde{\lambda}_j + \mathcal{O}(\epsilon^{k+1}), \\ \tilde{\mathbf{v}}^{(1)}(\epsilon) &= \sum_{j=0}^k \epsilon^j \tilde{\mathbf{v}}_j + \mathcal{O}(\epsilon^{k+1}), \\ \tilde{\mathbf{u}}^{(1)}(\epsilon) &= \sum_{j=0}^k \epsilon^j \tilde{\mathbf{u}}_j + \mathcal{O}(\epsilon^{k+1}). \end{aligned}$$

We use superscripts to indicate powers of ϵ in the terms in the expansion and subscripts for the terms that are multiplied by ϵ^j . Note that $\tilde{\lambda}_0$, $\tilde{\mathbf{v}}_0$, and $\tilde{\mathbf{u}}_0$, respectively, indicate the dominant eigenvalue and corresponding right and left eigenvectors in the limit $\epsilon \rightarrow 0^+$. Successive terms in these expansions represent higher-order derivatives, and each term assumes appropriate smoothness of these functions.

Our strategy is to develop consistent solutions to $\tilde{\mathbf{C}}(\epsilon)^T \tilde{\mathbf{u}}(\epsilon) = \tilde{\lambda}_{\max}(\epsilon) \tilde{\mathbf{u}}(\epsilon)$ and $\tilde{\mathbf{C}}(\epsilon) \tilde{\mathbf{v}}(\epsilon) = \tilde{\lambda}_{\max}(\epsilon) \tilde{\mathbf{v}}(\epsilon)$ for progressively larger values of k . Starting with the first-order approximation, we insert $\tilde{\lambda}_{\max}(\epsilon) \approx \tilde{\lambda}_0 + \epsilon \tilde{\lambda}_1$ and $\tilde{\mathbf{v}}(\epsilon) \approx \tilde{\mathbf{v}}_0 + \epsilon \tilde{\mathbf{v}}_1$ into Eq. (3.2) and collect the zeroth-order and first-order terms in ϵ to obtain

$$(E.2) \quad (\tilde{\lambda}_0 \mathbb{I} - \hat{\mathbf{A}}) \tilde{\mathbf{v}}_0 = 0,$$

$$(E.3) \quad (\tilde{\lambda}_0 \mathbb{I} - \hat{\mathbf{A}}) \tilde{\mathbf{v}}_1 = (\hat{\mathbf{C}} - \tilde{\lambda}_1 \mathbb{I}) \tilde{\mathbf{v}}_0,$$

where \mathbb{I} is the $NT \times NT$ identity matrix. Equation (E.2) corresponds to the system described by Thm. 4.1, implying that the operator $\tilde{\lambda}_0 \mathbb{I} - \hat{\mathbf{A}}$ is singular and has an N -dimensional null space. (This is the dominant eigenspace of $\hat{\mathbf{A}}$.) Specifically, Eq. (E.2) has a general solution of the form

$$(E.4) \quad \begin{aligned} \tilde{\mathbf{v}}_0 &= \sum_j \tilde{\alpha}_j \mathbb{P} \tilde{\mathbf{v}}^{(1,j)}, \\ \tilde{\lambda}_0 &= \max_t \tilde{\mu}_t, \end{aligned}$$

where $\{\tilde{\alpha}_i\}$ are constants that satisfy $\sum_i \tilde{\alpha}_i^2 = 1$, so that $\|\tilde{\mathbf{v}}_0\|_2 = 1$. Additionally,

$$(E.5) \quad \tilde{\mathbf{u}}_0 = \sum_j \tilde{\beta}_j \mathbb{P} \tilde{\mathbf{u}}^{(1,j)},$$

where $\sum_i \tilde{\beta}_i^2 = 1$, so that $\|\tilde{\mathbf{u}}_0\|_2 = 1$.

To determine the vectors $\tilde{\boldsymbol{\alpha}} = [\tilde{\alpha}_1, \dots, \tilde{\alpha}_N]^T$ and $\tilde{\boldsymbol{\beta}} = [\tilde{\beta}_1, \dots, \tilde{\beta}_N]^T$ of constants that uniquely determine $\tilde{\mathbf{u}}_0$ and $\tilde{\mathbf{v}}_0$, we seek a solvability condition in the first-order terms. Using the fact that the left null space of $\tilde{\lambda}_0 \mathbb{I} - \hat{\mathbf{A}}$ is the span of $\{\mathbb{P} \tilde{\mathbf{u}}^{(1,i)}\}$, it follows that $[\tilde{\mathbf{u}}^{(1,i)}]^T \mathbb{P}^T (\tilde{\lambda}_0 \mathbb{I} - \hat{\mathbf{A}}) \tilde{\mathbf{v}}_1 = 0$. Therefore, we left-multiply Eq. (E.3) by $[\tilde{\mathbf{u}}^{(1,i)}]^T \mathbb{P}^T$ and simplify to obtain

$$(E.6) \quad [\tilde{\mathbf{u}}^{(1,i)}]^T \mathbb{P}^T \hat{\mathbf{C}} \tilde{\mathbf{v}}_0 = \tilde{\lambda}_1 [\tilde{\mathbf{u}}^{(1,i)}]^T \mathbb{P}^T \tilde{\mathbf{v}}_0.$$

Using the solution of $\tilde{\mathbf{v}}_0$ in Eq. (E.4), we obtain

$$\begin{aligned}
 \sum_j \tilde{\alpha}_j [\tilde{\mathbf{u}}^{(1,i)}]^T \mathbb{P}^T \hat{\mathbb{C}} \mathbb{P} \tilde{\mathbf{v}}^{(1,j)} &= \tilde{\lambda}_1 \sum_j \tilde{\alpha}_j [\tilde{\mathbf{u}}^{(1,i)}]^T \mathbb{P}^T \mathbb{P} \tilde{\mathbf{v}}^{(1,j)} \\
 &= \tilde{\lambda}_1 \sum_j \tilde{\alpha}_j [\tilde{\mathbf{u}}^{(1,i)}]^T \tilde{\mathbf{v}}^{(1,j)} \\
 (E.7) \qquad \qquad \qquad &= \tilde{\lambda}_1 \langle \tilde{\mathbf{u}}^{(1)}, \tilde{\mathbf{v}}^{(1)} \rangle \tilde{\alpha}_i,
 \end{aligned}$$

because $\mathbb{P}^T \mathbb{P} = \mathbb{P} \mathbb{P}^T = \mathbb{I}$ and $[\tilde{\mathbf{u}}^{(1,i)}]^T \tilde{\mathbf{v}}^{(1,j)} = \langle \tilde{\mathbf{u}}^{(1)}, \tilde{\mathbf{v}}^{(1)} \rangle \delta_{ij}$, where δ_{ij} is the Kronecker delta. We divide by Eq. (E.7) by $\langle \tilde{\mathbf{u}}^{(1)}, \tilde{\mathbf{v}}^{(1)} \rangle$ to obtain an N -dimensional eigenvalue equation for the dominant eigenvector $\tilde{\alpha}$. One can implement the analogous steps for the left dominant eigenvector equations, and together these two eigenvector equations yield Eq. (4.11).

REFERENCES

- [1] W. AHMAD, M. A. PORTER, AND M. BEGUERISSE-DÍAZ, *Tie-decay temporal networks in continuous time and eigenvector-based centralities*, arXiv preprint arXiv:1805.00193, (2018).
- [2] A. ALSAYED AND D. J. HIGHAM, *Betweenness in time dependent networks*, *Chaos, Solitons & Fractals*, 72 (2015), pp. 35–48.
- [3] F. ARRIGO AND D. J. HIGHAM, *Sparse matrix computations for dynamic network centrality*, *Applied Network Science*, 2 (2017), p. 17.
- [4] R. B. BAPAT AND T. E. S. RAGHAVAN, *Nonnegative Matrices and Applications*, vol. 64, Cambridge University Press, 1997.
- [5] M. BARDOSCIA, G. BIANCONI, AND G. FERRARA, *Multiplex network analysis of the UK OTC derivatives market*, (2018). Preprint, available at https://papers.ssrn.com/sol3/papers.cfm?abstract_id=3180709.
- [6] D. S. BASSETT, N. F. WYMBES, M. P. ROMBACH, M. A. PORTER, P. J. MUCHA, AND S. T. GRAFTON, *Task-based core-periphery organization of human brain dynamics*, *PLoS computational biology*, 9 (2013), p. e1003171.
- [7] F. BATTISTON, V. NICOSIA, AND V. LATORA, *Structural measures for multiplex networks*, *Physical Review E*, 89 (2014), p. 032804.
- [8] G. BIANCONI, *Multilayer Networks: Structure and Function*, Oxford University Press, 2018.
- [9] S. BOCCALETTI, G. BIANCONI, R. CRIADO, C.I. DEL GENIO, J. GÓMEZ-GARDEÑES, M. ROMANCE, I. SENDINA-NADAL, Z. WANG, AND M. ZANIN, *The structure and dynamics of multilayer networks*, *Physics Reports*, 544 (2014), pp. 1–122.
- [10] P. BONACICH, *Factoring and weighting approaches to clique identification*, *Journal of Mathematical Sociology*, 2 (1972), pp. 113–120.
- [11] S. BRIN AND L. PAGE, *Anatomy of a large-scale hypertextual web search engine*, *Proceedings of the Seventh International World Wide Web Conference*, (1998), pp. 107–117.
- [12] T. CALLAGHAN, M. A. PORTER, AND P. J. MUCHA, *Random walker ranking for NCAA Division I-A football*, *American Mathematical Monthly*, 114 (2007), pp. 761–777.
- [13] A. CARDILLO, J. GÓMEZ-GARDENES, M. ZANIN, M. ROMANCE, D. PAPO, F. DEL POZO, AND S. BOCCALETTI, *Emergence of network features from multiplexity*, *Scientific Reports*, 3 (2013), p. 1344.
- [14] T. CHAKRABORTY AND R. NARAYANAM, *Cross-layer betweenness centrality in multiplex networks with applications*, in *Data Engineering (ICDE)*, 2016 IEEE 32nd International Conference on, IEEE, 2016, pp. 397–408.
- [15] T. P. CHARTIER, E. KREUTZER, A. N. LANGVILLE, AND K. E. PEDINGS, *Sensitivity and stability of ranking vectors*, *SIAM Journal on Scientific Computing*, 33 (2011), pp. 1077–1102.
- [16] I. CHEN, M. BENZI, H. H. CHANG, AND V. S. HERTZBERG, *Dynamic communicability and epidemic spread: A case study on an empirical dynamic contact network*, *Journal of Complex Networks*, 5 (2016), pp. 274–302.

- [17] M. COSCIA, G. ROSSETTI, D. PENNACCHIOLI, D. CECCARELLI, AND F. GIANNOTTI, *You know because i know: a multidimensional network approach to human resources problem*, in Proceedings of the 2013 IEEE/ACM International Conference on Advances in Social Networks Analysis and Mining, ACM, 2013, pp. 434–441.
- [18] E. COZZO, G. FERRAZ DE ARRUDA, F. A. RODRIGUES, AND Y. MORENO, *Multiplex Networks: Basic Formalism and Structural Properties*, Springer-Verlag, 2018.
- [19] C. DE BACCO, D. B. LARREMORE, AND C. MOORE, *A physical model for efficient ranking in networks*, *Science advances*, 4 (2018), p. eaar8260.
- [20] M. DE DOMENICO, S. SASAI, AND A. ARENAS, *Mapping multiplex hubs in human functional brain networks*, *Frontiers in Neuroscience*, 10 (2016), p. 326.
- [21] M. DE DOMENICO, A. SOLÉ-RIBALTA, E. COZZO, M. KIVELÄ, Y. MORENO, M. A. PORTER, S. GÓMEZ, AND A. ARENAS, *Mathematical formulation of multilayer networks*, *Physical Review X*, 3 (2013), p. 041022.
- [22] M. DE DOMENICO, A. SOLÉ-RIBALTA, E. OMODEI, S. GÓMEZ, AND A. ARENAS, *Ranking in interconnected multilayer networks reveals versatile nodes*, *Nature Communications*, 6 (2015), p. 6868.
- [23] D. R. DEFORD, *Multiplex dynamics on the World Trade Web*, in International Workshop on Complex Networks and their Applications, Springer, 2017, pp. 1111–1123.
- [24] D. R. DEFORD AND S. D. PAULS, *A new framework for dynamical models on multiplex networks*, *Journal of Complex Networks*, 6 (2017), pp. 353–381.
- [25] C. DING AND K. LI, *Centrality ranking in multiplex networks using topologically biased random walks*, *Neurocomputing*, (2018).
- [26] E. ESTRADA, *Communicability in temporal networks*, *Physical Review E*, 88 (2013), p. 042811.
- [27] M. G. EVERETT AND S. P. BORGATTI, *Networks containing negative ties*, *Social Networks*, 38 (2014), pp. 111–120.
- [28] C. FENU AND D. J. HIGHAM, *Block matrix formulations for evolving networks*, *SIAM Journal of Matrix Analysis and Applications*, 38 (2017), pp. 343–360.
- [29] J. FLORES AND M. ROMANCE, *On eigenvector-like centralities for temporal networks: Discrete vs. continuous time scales*, *Journal of Computational and Applied Mathematics*, 330 (2018), pp. 1041–1051.
- [30] S. FORTUNATO, C. T. BERGSTROM, K. BÖRNER, J. A. EVANS, D. HELBING, S. MILOJEVIĆ, A. M. PETERSEN, F. RADICCHI, R. SINATRA, B. UZZI, A. VESPIGNANI, L. WALTMAN, D. WANG, AND A.-L. BARABÁSI, *Science of science*, 359 (2018).
- [31] J. H. FOWLER, T. R. JOHNSON, J. F. SPRIGGS II, S. JEON, AND P. J. WAHLBECK, *Network analysis and the law: Measuring the legal importance of precedents at the US Supreme Court*, *Political Analysis*, 15 (2007), pp. 324–346.
- [32] D. F. GLEICH, *PageRank beyond the Web*, *SIAM Review*, 57 (2015), pp. 321–363.
- [33] G. H. GOLUB AND C. F. VAN LOAN, *Matrix Computations*, Johns Hopkins University Press, third ed., 2012.
- [34] S. GÓMEZ, A. DÍAZ-GUILERA, J. GÓMEZ-GARDEÑES, C. J. PÉREZ-VICENTE, Y. MORENO, AND A. ARENAS, *Diffusion dynamics on multiplex networks*, *Physical Review Letters*, 110 (2013), p. 028701.
- [35] P. GONÇALVES, *Behavior modes, pathways and overall trajectories: Eigenvector and eigenvalue analysis of dynamic systems*, *System Dynamics Review: The Journal of the System Dynamics Society*, 25 (2009), pp. 35–62.
- [36] P. GRINDROD AND D. J. HIGHAM, *A matrix iteration for dynamic network summaries*, *SIAM Review*, 55 (2013), pp. 118–128.
- [37] ———, *A dynamical systems view of network centrality*, *Proceedings of the Royal Society A*, 470 (2014), p. 20130835.
- [38] P. GRINDROD, M. C. PARSONS, D. J. HIGHAM, AND E. ESTRADA, *Communicability across evolving networks*, *Physical Review E*, 83 (2011), p. 046120.
- [39] R. GUIMERÀ, S. MOSSA, A. TURTSCHI, AND L. A. N. AMARAL, *The worldwide air transportation network: Anomalous centrality, community structure, and cities' global roles*, *Proceedings of the National Academy of Sciences of the USA*, 102 (2005), pp. 7794–7799.
- [40] Y. Y. HAIMES AND P. JIANG, *Leontief-based model of risk in complex interconnected infrastructures*,

- Journal of Infrastructure systems, 7 (2001), pp. 1–12.
- [41] A. HALU, R. J. MONDRAGÓN, P. PANZARASA, AND G. BIANCONI, *Multiplex pagerank*, PLoS ONE, 8 (2013), p. e78293.
- [42] P. HOLME, *Congestion and centrality in traffic flow on complex networks*, Advances in Complex Systems, 6 (2003), pp. 163–176.
- [43] ———, *Modern temporal network theory: A colloquium*, European Physical Journal B, 88 (2015), p. 234.
- [44] P. HOLME AND J. SARAMÄKI, *Temporal networks*, Physics Reports, 519 (2012), pp. 97–125.
- [45] D.-W. HUANG AND Z.-G. YU, *Dynamic-sensitive centrality of nodes in temporal networks*, Scientific Reports, 7 (2017), p. 41454.
- [46] Q. HUANG, C. ZHAO, X. ZHANG, X. WANG, AND D. YI, *Centrality measures in temporal networks with time series analysis*, EPL (Europhysics Letters), 118 (2017), p. 36001.
- [47] J. IACOVACCI, C. RAHMEDE, A. ARENAS, AND G. BIANCONI, *Functional multiplex pagerank*, EPL (Europhysics Letters), 116 (2016), p. 28004.
- [48] H. JEONG, S. P. MASON, A.-L. BARABÁSI, AND Z. N. OLTVAI, *Lethality and centrality in protein networks*, Nature, 411 (2001), pp. 41–42.
- [49] C. E. KAMPMANN, *Feedback loop gains and system behavior*, in Proceedings of the 1996 International System Dynamics Conference, System Dynamics Society Cambridge, MA, 1996, pp. 21–25.
- [50] C. E. KAMPMANN AND R. OLIVA, *Loop eigenvalue elasticity analysis: three case studies*, System Dynamics Review: The Journal of the System Dynamics Society, 22 (2006), pp. 141–162.
- [51] D. KEMPE, J. KLEINBERG, AND É. TARDOS, *Maximizing the spread of influence through a social network*, in Proceedings of the ninth ACM SIGKDD international conference on Knowledge discovery and data mining, ACM, 2003, pp. 137–146.
- [52] H. KIM, J. TANG, R. ANDERSON, AND C. MASCOLO, *Centrality prediction in dynamic human contact networks*, Computer Networks, 56 (2012), pp. 983–996.
- [53] M. KIVELÄ, A. ARENAS, M. BARTHELEMY, J. P. GLEESON, Y. MORENO, AND M. A. PORTER, *Multi-layer networks*, Journal of Complex Networks, 2 (2014), pp. 203–271.
- [54] M. KIVELÄ AND M. A. PORTER, *Isomorphisms in multilayer networks*, Transactions on Network Science and Engineering, 5 (2018), pp. 198–211.
- [55] J. KLEINBERG, *Authoritative sources in a hyperlinked environment*, Journal of the ACM (JACM), 46 (1999), pp. 604–632.
- [56] T. KOLDA AND B. BADER, *The TOPHITS model for higher-order Web link analysis*, in Workshop on Link Analysis, Counterterrorism and Security, vol. 7, 2006, pp. 26–29.
- [57] D. KRACKHARDT, *Cognitive social structures*, Social networks, 9 (1987), pp. 109–134.
- [58] A. N. LANGVILLE AND C. D. MEYER, *Google’s PageRank and Beyond: The Science of Search Engine Rankings*, Princeton University Press, 2006.
- [59] E. A. LEICHT, G. CLARKSON, K. SHEDDEN, AND M. E. J. NEWMAN, *Large-scale structure of time evolving citation networks*, The European Physical Journal B, 59 (2007), pp. 75–83.
- [60] K. LERMAN, R. GHOSH, AND J. H. KANG, *Centrality metric for dynamic networks*, in Proceedings of the Eighth Workshop on Mining and Learning with Graphs, ACM, 2010, pp. 70–77.
- [61] H. LIAO, M. S. MARIANI, M. MEDO, Y.-C. ZHANG, AND M.-Y. ZHOU, *Ranking in evolving complex networks*, Physics Reports, 689 (2017), pp. 1–54.
- [62] N. LOTFI, A. H. DAROONEH, AND F. A. RODRIGUES, *Centrality in earthquake multiplex networks*, Chaos, 28 (2018), p. 063113.
- [63] M. MAGNANI, B. MICENKOVA, AND L. ROSSI, *Combinatorial analysis of multiple networks*, arXiv preprint arXiv:1303.4986, (2013).
- [64] M. MAGNANI AND L. ROSSI, *The ml-model for multi-layer social networks*, in Advances in Social Networks Analysis and Mining (ASONAM), 2011 International Conference on, IEEE, 2011, pp. 5–12.
- [65] A. V. MANTZARIS, D. S BASSETT, N. F. WYMBS, E. ESTRADA, M. A. PORTER, P. J. MUCHA, S. T. GRAFTON, AND D. J. HIGHAM, *Dynamic network centrality summarizes learning in the human brain*, Journal of Complex Networks, 1 (2013), pp. 83–92.
- [66] A. V. MANTZARIS AND D. J. HIGHAM, *Dynamic communicability predicts infectiousness*, in Temporal Networks, Springer, 2013, pp. 283–294.
- [67] T. MARTIN, X. ZHANG, AND M. E. J. NEWMAN, *Localization and centrality in networks*, Physical Review E, 90 (2014), p. 052808.

- [68] S. MOTEGI AND N. MASUDA, *A network-based dynamical ranking system for competitive sports*, Scientific Reports, 2 (2012).
- [69] P. J. MUCHA, T. RICHARDSON, K. MACON, M. A. PORTER, AND J.-P. ONNELA, *Community structure in time-dependent, multiscale, and multiplex networks*, Science, 328 (2010), pp. 876–878.
- [70] E. NATHAN, J. FAIRBANKS, AND D. BADER, *Ranking in dynamic graphs using exponential centrality*, in International Workshop on Complex Networks and their Applications, Springer, 2017, pp. 378–389.
- [71] H. NAYAR, B. A. MILLER, K. GEYER, R. S. CACERES, S. T. SMITH, AND R. R. NADAKUDITI, *Improved hidden clique detection by optimal linear fusion of multiple adjacency matrices*, in Signals, Systems and Computers, 2015 49th Asilomar Conference on, IEEE, 2015, pp. 1520–1524.
- [72] M. E. J. NEWMAN, *Networks*, Oxford University Press, second ed., 2018.
- [73] M. K.-P. NG, X. LI, AND Y. YE, *Multirank: co-ranking for objects and relations in multi-relational data*, in Proceedings of the 17th ACM SIGKDD international conference on Knowledge discovery and data mining, ACM, 2011, pp. 1217–1225.
- [74] N. OTTER, M. A. PORTER, U. TILLMANN, P. GRINDROD, AND H. A. HARRINGTON, *A roadmap for the computation of persistent homology*, European Physical Journal — Data Science, 6 (2017), pp. 1–38.
- [75] L. PAGE, S. BRIN, R. MOTWANI, AND T. WINOGRAD, *The PageRank citation ranking: Bringing order to the Web*, (1999).
- [76] A. R. PAMPIL, S. D. HOWISON, R. LAMBIOTTE, AND M. A. PORTER, *Relating modularity maximization and stochastic block models in multilayer networks*, arXiv preprint arXiv:1804.01964, (2018).
- [77] R. PAN AND J. SARAMÄKI, *Path lengths, correlations, and centrality in temporal networks*, Physical Review E, 84 (2011).
- [78] R. PASTOR-SATORRAS AND C. CASTELLANO, *Eigenvector localization in real networks and its implications for epidemic spreading*, Journal of Statistical Physics, (2018), pp. 1–14.
- [79] M. A. PORTER, *What is... a multilayer network*, Notices of the American Mathematical Society, in press (December issue) (2018).
- [80] MÁRTON PÓSFAL, NIKLAS BRAUN, BRIANNE A BEISNER, BRENDA MCCOWAN, AND RAISSA M D’SOUZA, *Consensus ranking for multi-objective interventions in multiplex networks*, arXiv preprint arXiv:1903.02059, (2019).
- [81] S. PRAPROTNIK AND V. BATAGELJ, *Spectral centrality measures in temporal networks*, Ars Mathematica Contemporanea, 11 (2015), pp. 11–33.
- [82] MATHEMATICS GENEALOGY PROJECT, *The Mathematics Genealogy Project*, 2009. <http://www.genealogy.ams.org>, data provided 19 October 2009.
- [83] F. RADICCHI AND A. ARENAS, *Abrupt transition in the structural formation of interconnected networks*, Nature Physics, 9 (2013), p. 717.
- [84] C. RAHMEDE, J. IACOVACCI, A. ARENAS, AND G. BIANCONI, *Centralities of nodes and influences of layers in large multiplex networks*, Journal of Complex Networks, (2017).
- [85] A. REIFFERS-MASSON AND V. LABATUT, *Opinion-based centrality in multiplex networks: A convex optimization approach*, Network Science, 5 (2017), pp. 213–234.
- [86] J. G. RESTREPO, E. OTT, AND B. R. HUNT, *Characterizing the dynamical importance of network nodes and links*, Physical Review Letters, 97 (2006), p. 094102.
- [87] L. E. C. ROCHA AND N. MASUDA, *Random walk centrality for temporal networks*, New Journal of Physics, 16 (2014), p. 063023.
- [88] M. ROMANCE, L. SOLÁ, J. FLORES, E. GARCÍA, A. G. DEL AMO, AND R. CRIADO, *A Perron–Frobenius theory for block matrices associated to a multiplex network*, Chaos, Solitons & Fractals, 72 (2015), pp. 77–89.
- [89] R. A. ROSSI AND D. F. GLEICH, *Dynamic PageRank using evolving teleportation*, in Algorithms and Models for the Web Graph, Springer, 2012, pp. 126–137.
- [90] S. SAAVEDRA, S. POWERS, T. MCCOTTER, M. A. PORTER, AND P. J. MUCHA, *Mutually-antagonistic interactions in baseball networks*, Physica A, 389 (2010), pp. 1131–1141.
- [91] L. SOLÁ, M. ROMANCE, R. CRIADO, J. FLORES, A. G. DEL AMO, AND S. BOCCALETTI, *Eigenvector centrality of nodes in multiplex networks*, Chaos, 23 (2013), p. 033131.
- [92] A. SOLÉ-RIBALTA, M. DE DOMENICO, S. GÓMEZ, AND A. ARENAS, *Centrality rankings in multiplex networks*, in Proceedings of the 2014 ACM Conference on Web Science, ACM, 2014, pp. 149–155.
- [93] ———, *Random walk centrality in interconnected multilayer networks*, Physica D, 323 (2016), pp. 73–79.

- [94] A. SOLÉ-RIBALTA, M. DE DOMENICO, N. E. KOUVARIS, A. DIAZ-GUILERA, S. GOMEZ, AND A. ARENAS, *Spectral properties of the Laplacian of multiplex networks*, *Physical Review E*, 88 (2013), p. 032807.
- [95] C. SPATOCCO, G. STILO, AND C. DOMENICONI, *A new framework for centrality measures in multiplex networks*, arXiv preprint arXiv:1801.08026, (2018).
- [96] T. TAKAGUCHI, Y. YANO, AND Y. YOSHIDA, *Coverage centralities for temporal networks*, *The European Physical Journal B*, 89 (2016), pp. 1–11.
- [97] J. TANG, M. MUSOLESI, C. MASCOLO, V. LATORA, AND V. NICOSIA, *Analysing information flows and key mediators through temporal centrality metrics*, in Proc. of the 3rd Workshop on Social Network Systems - SNS '10, 2010, pp. 1–6.
- [98] S. TAVASSOLI AND K. A. ZWEIG, *Most central or least central? how much modeling decisions influence a node's centrality ranking in multiplex networks*, arXiv preprint arXiv:1606.05468, (2016).
- [99] D. TAYLOR, *Code release: Supracentrality* <https://github.com/taylordr/Supracentrality>.
- [100] ———, *Data release: Ph.D. exchange in the Mathematical Genealogy Project* <https://sites.google.com/site/danetaylorresearch/home/data>.
- [101] D. TAYLOR AND D. B. LARREMORE, *Social climber attachment in forming networks produces a phase transition in a measure of connectivity*, *Physical Review E*, 86 (2012), p. 031140.
- [102] D. TAYLOR, S. A. MYERS, A. CLAUSET, M. A. PORTER, AND P. J. MUCHA, *Eigenvector-based centrality measures for temporal networks*, *Multiscale Modeling & Simulation*, 15 (2017), pp. 537–574.
- [103] D. TAYLOR AND J. G. RESTREPO, *Network connectivity during mergers and growth: Optimizing the addition of a module*, *Physical Review E*, 83 (2011), p. 066112.
- [104] ———, *A network-specific approach to percolation in complex networks with bidirectional links*, *EPL (Europhysics Letters)*, 98 (2012), p. 16007.
- [105] D. TAYLOR, P. S. SKARDAL, AND J. SUN, *Synchronization of heterogeneous oscillators under network modifications: Perturbation and optimization of the synchrony alignment function*, *SIAM Journal on Applied Mathematics*, 76 (2016), pp. 1984–2008.
- [106] H. TONG, B. A. PRAKASH, T. ELIASSI-RAD, M. FALOUTSOS, AND C. FALOUTSOS, *Gelling, and melting, large graphs by edge manipulation*, in Proceedings of the 21st ACM international conference on Information and knowledge management, ACM, 2012, pp. 245–254.
- [107] F. TUDISCO, F. ARRIGO, AND A. GAUTIER, *Node and layer eigenvector centralities for multiplex networks*, *SIAM Journal on Applied Mathematics*, 78 (2018), pp. 853–876.
- [108] M. VAIANA AND S. F. MULDOON, *Multilayer brain networks*, *Journal of Nonlinear Science*, (2018).
- [109] E. VALDANO, L. FERRERI, C. POLETO, AND V. COLIZZA, *Analytical computation of the epidemic threshold on temporal networks*, *Physical Review X*, 5 (2015), p. 021005.
- [110] W. H. WEIR, S. EMMONS, R. GIBSON, D. TAYLOR, AND P. J. MUCHA, *Post-processing partitions to identify domains of modularity optimization*, *Algorithms*, 10 (2017), p. 93.
- [111] M. J. WILLIAMS AND M. MUSOLESI, *Spatio-temporal networks: Reachability, centrality and robustness*, *Royal Society Open Science*, 3 (2016).
- [112] K. YOU, R. TEMPO, AND L. QIU, *Distributed algorithms for computation of centrality measures in complex networks*, *IEEE Transactions on Automatic Control*, 62 (2017), pp. 2080–2094.
- [113] M. YU, M. ENGELS, A. HILLEBRAND, E. CW VAN STRAATEN, A. A. GOUW, C. TEUNISSEN, W. M. VAN DER FLIER, P. SCHELTENS, AND C. J. STAM, *Selective impairment of hippocampus and posterior hub areas in Alzheimer's disease: An MEG-based multiplex network study*, *Brain*, 140 (2017), pp. 1466–1485.

SUPPLEMENTARY MATERIALS: Tunable Eigenvector-Based Centralities for Multiplex and Temporal Networks *

Dane Taylor[†], Mason A. Porter[‡], and Peter J. Mucha[§]

In this supplement, we provide more details about our pedagogical example and our two case studies of empirical data sets.

SM1. Extended Study of the Pedagogical Example. In this section, we present an extended study of our numerical experiment (see Sec. 3.3 of the main text) in which we examined the multiplex network in Fig. 1(a). Recall for this network that the interlayer coupling between layers 3 and 4 have a different coupling than that of the other interlayer couplings. (See the dashed lines in Fig. 1(a).) In Sec. 3.3, we set $\tilde{A}_{34} = \tilde{A}_{43} = 0.01$, whereas we set $\tilde{A}_{tt'} = 1$ for the other interlayer couplings.

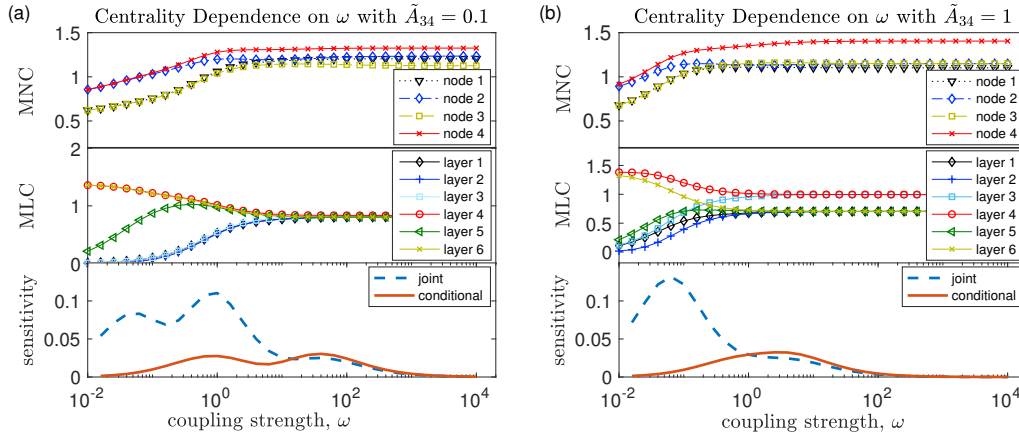


Figure SM1. Supracentrality results for our pedagogical multiplex network in which the coupling between layers 3 and 4 is different than the coupling between the other layers. In panels (a) and (b), we report the same results as in Fig. 3(b) in the main text (which used $\tilde{A}_{34} = \tilde{A}_{43} = 0.01$), except that we now use (a) $\tilde{A}_{34} = \tilde{A}_{43} = 0.1$ and (b) $\tilde{A}_{34} = \tilde{A}_{43} = 1$. Note in panel (b) that the curves for sensitivity, as measured by the stepwise magnitude of change, $\|\mathbf{W}(\omega_s) - \mathbf{W}(\omega_{s-1})\|_F$ and $\|\mathbf{Z}(\omega_s) - \mathbf{Z}(\omega_{s-1})\|_F$, are no longer bimodal.

In Fig. SM1, we now explore two other choices: (a) $\tilde{A}_{34} = \tilde{A}_{43} = 0.1$ and (b) $\tilde{A}_{34} = \tilde{A}_{43} = 1$. We now plot the marginal node centralities (MNCs), marginal layer centralities (MLCs), and sensitivity of the joint and conditional centralities — as measured by the stepwise magnitude of change, $\|\mathbf{W}(\omega_s) - \mathbf{W}(\omega_{s-1})\|_F$ and $\|\mathbf{Z}(\omega_s) - \mathbf{Z}(\omega_{s-1})\|_F$ — across a range of coupling strengths ω . Note in panel (b) that the curves are no longer bimodal, implying that

*

[†]Department of Mathematics, University at Buffalo, State University of New York, Buffalo, NY 14260, USA

[‡]Department of Mathematics, University of California, Los Angeles, CA 90095, USA

[§]Carolina Center for Interdisciplinary Applied Mathematics, Department of Mathematics and Department of Applied Physical Sciences, University of North Carolina, Chapel Hill, NC 27599, USA

SM1

a stable intermediate regime vanishes as we increase \tilde{A}_{34} . Intuitively, this occurs because the network associated with the interlayer adjacency matrix $\tilde{\mathbf{A}}$ shown in Fig. 1(a) no longer has two well-separated communities if $\tilde{A}_{34} = \tilde{A}_{43} = 1$.

Table SM1

List of European airline companies, which we represent as layers in a multiplex network. For each layer, we report the number M_t of undirected edges and the spectral radius $\lambda_1^{(t)}$ of its associated adjacency matrix $\mathbf{A}^{(t)}$.

Layer (t)	Airline Name	M_t	$\lambda_1^{(t)}$	Layer t	Airline Name	M_t	$\lambda_1^{(t)}$
1	Lufthansa	244	14.5	20	LOT Polish Air.	55	6.8
2	Ryanair	601	19.3	21	Vueling Airlines	63	6.8
3	Easyjet	307	14.0	22	Air Nostrum	69	6.4
4	British Airways	66	6.6	23	Air Lingus	108	6.7
5	Turkish Airlines	118	9.9	24	Germanwings	67	7.4
6	Air Berlin	184	11.3	25	Pegasus Airlines	58	6.7
7	Air France	69	7.2	26	Netjets	180	8.2
8	Scandinavian Air.	110	8.9	27	Transavia Holland	57	6.0
9	KLM	62	7.9	28	Niki	37	4.7
10	Alitalia	93	8.8	29	SunExpress	67	7.8
11	Swiss Int. Air Lines	60	7.3	30	Aegean Airlines	53	6.5
12	Iberia	35	5.8	31	Czech Airlines	41	6.4
13	Norwegian Air Shu.	67	8.1	32	European Air Trans.	73	6.8
14	Austrian Airlines	74	8.1	33	Malev Hungarian Air.	34	5.8
15	Flybe	99	8.5	34	Air Baltic	45	6.4
16	Wizz Air	92	6.5	35	Wideroe	40	5.6
17	TAP Portugal	53	7.0	36	TNT Airways	61	6.2
18	Brussels Airlines	43	6.6	37	Olympic Air	43	6.2
19	Finnair	42	6.4				

SM2. Extended Study of European Airport Rankings. In this section, we discuss additional results for our study of European airline transportation, which we presented in Sec. 5.1 of the main text. Recall that the network has $N = 417$ European airports, which we identify to be in the largest strongly connected component of the multiplex network (identified after summing the layers' adjacency matrices). There are $T = 37$ layers, each representing the flight patterns between airports for a single airline company. In Table SM1, we list these airline companies. For each layer, we indicate the number $M_t = \frac{1}{2} \sum_{ij} A_{ij}^{(t)}$ of intralayer edges and the spectral radius $\lambda_1^{(t)}$ of the layer's associated adjacency matrix $\mathbf{A}^{(t)}$. The layer that represents Ryanair ($t = 2$) has the most edges, with almost twice as many as any other airline, and the largest spectral radius. In Sec. 5.1 of main text, we studied supracentralities for the multiplex network using the layers' adjacency matrices as their centrality matrices, $\mathbf{C}^{(t)} = \mathbf{A}^{(t)}$, and found that the Ryanair network dominates the supracentralities in the weak-coupling limit due to an eigenvector localization phenomenon in which $\mathbf{v}(\omega)$ localizes onto layer $t = 2$. (See Fig. 4(a) of the main text.) Corollary 4.3 describes this phenomenon, which occurs because the centrality matrix for Ryanair has the largest spectral radius.

We now study supracentralities when the layers' centrality matrices are PageRank matrices (see Definition 2.5 in the main text). In Table SM2, we list the airports having the

SM2

Table SM2

European airports with the top MNCs for coupling strengths $\omega \in \{0.01, 1, 100\}$, which correspond to the regimes of weak, intermediate, and strong coupling. We show results are for when the layers' centrality matrices are PageRank matrices and the interlayer adjacency matrix is $\mathbf{A} = \mathbf{1}\mathbf{1}^T$. We indicate airports by their International Civil Aviation Organization (ICAO) codes.

Rank	$\omega = 10^{-4}$		$\omega = 10^{-1}$		$\omega = 10^2$	
	Airport	MNC	Airport	MNC	Airport	MNC
1	EHAM	0.406	LTBA	0.802	LTBA	0.929
2	LOWW	0.373	EBLG	0.732	EBLG	0.866
3	LTBA	0.372	LTFJ	0.700	EVRA	0.818
4	EGKK	0.365	EVRA	0.695	LTFJ	0.791
5	LEMD	0.363	EHAM	0.662	EHAM	0.725
6	LTFJ	0.344	EGKK	0.653	LOWW	0.699
7	LFPG	0.337	LOWW	0.633	EGKK	0.698
8	LGAV	0.333	EIDW	0.586	EIDW	0.656
9	EGLL	0.328	EGSS	0.583	EGSS	0.631
10	EIDW	0.328	LEMD	0.554	LEMD	0.596

highest MLC for small, intermediate, and large values of coupling strength ω . Unsurprisingly, there is some overlap with the top-ranked airports in Table 2 in the main text. For example, LEMD (Adolfo Suárez Madrid–Barajas Airport) makes the top-10 list for all ω values in both tables. However, most of the top-ranked airports are different. In particular, for $\omega \geq 0.1$ the top-ranked airports are LTBA, EBLG, LTFJ, and EVRA when using PageRank matrices, and none of these airports are in Table 2 of the main text. This is unsurprising, as it is well known for monolayer networks that PageRank and eigenvector centrality are correlated with each other, but they identify different types of node importances.

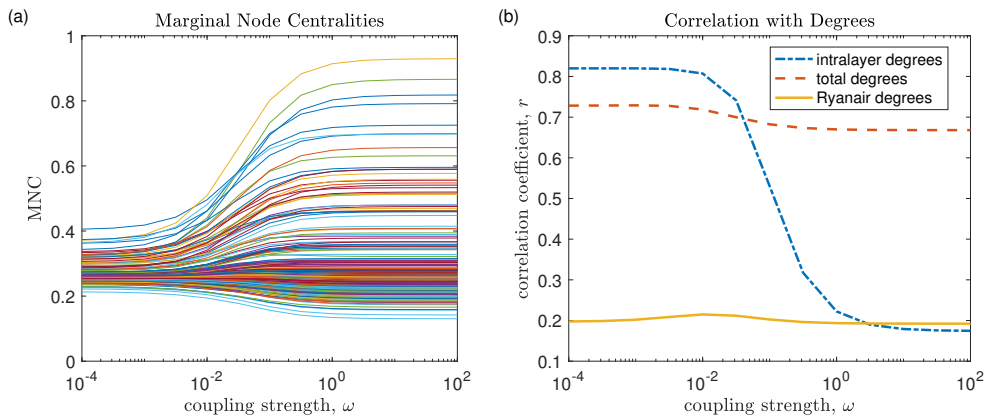


Figure SM2. Supracentralities for the multiplex European airline network with the layers' centrality matrices given by their PageRank matrices. (a) Airport MLCs versus intralayer coupling strength ω . (b) Pearson correlation coefficients for comparing supracentralities and node degrees (see the text).

One of the main causes for these differences can be seen by considering the limit of small

ω . In Fig. 5(b) of the main text, we observed that the marginal centralities correlated very strongly with the intralayer node degrees in the Ryanair layer, but not in other layers. However, as we can see in Fig. SM2(b), the PageRank MLCs paint a very different picture. Specifically, for small values of ω , the conditional centralities correlate strongly with the intralayer node degrees of all layers. In other words, for eigenvector supracentrality, the Ryanair layer dominates, and the supracentralities largely reflect the intralayer node degrees of this single layer. By contrast, for PageRank supracentralities, the Ryanair layer is not dominant. Whether there is such domination or not depends on whether there is eigenvector localization as $\omega \rightarrow 0^+$, as described by Thm. 4.2 and Cor. 4.3 of the main text. In this example, localization occurs for eigenvector supracentrality but not for PageRank supracentrality. Eigenvector localization does not occur in the latter case because PageRank matrices are transition matrices for Markov chains and thus have spectral radius equal to one.

SM3. Extended Study of United States Mathematical-Sciences Program Rankings.

In this section, we present additional results for our study (see Sec. 5.2 of the main text) of supracentralities in a temporal network of the graduation and hiring of mathematical-science Ph.D.s between U.S. universities. In Table SM3, we list the universities with top MNCs for when the layers' centrality matrices are given by their authority matrices (see Definition 2.4 in the main text). The interlayer adjacency matrix $\tilde{\mathbf{A}}$ is given by Eq. (5.5) of the main text. We show results for several choices of the layer-teleportation parameter γ and interlayer coupling strength ω . Observe that the particular ordering of the top-ranked schools depends sensitively on the choices for γ and ω ; however, we generally see the same set of universities near the top. MIT, for example, is almost always ranked first in the entire (γ, ω) parameter space.

Table SM3

Top MNC (see Definition 3.3 of the main text) for U.S. mathematics departments with the layers' centrality matrices given by authority matrices and the topology of interlayer coupling given by Eq. 5.5 of the main text. We show results for three choices of the layer-teleportation parameter γ and interlayer coupling strength ω .

Rank	MNC, $(\gamma, \omega) = (10^{-2}, 1)$		MNC, $(\gamma, \omega) = (10^{-2}, 10^2)$		MNC, $(\gamma, \omega) = (10^{-3}, 10^2)$	
	University	\hat{x}_i	University	\hat{x}_i	University	\hat{x}_i
1	MIT	0.91	MIT	5.28	MIT	3.47
2	U Washington	0.23	UC Berkeley	2.28	UC Berkeley	1.72
3	Boston U	0.15	Stanford	1.84	Stanford	1.28
4	U Michigan	0.12	Princeton	1.42	Harvard	0.97
5	Brown	0.12	Harvard	1.28	Princeton	0.96
6	UCLA	0.111	Cornell	1.23	Cornell	0.89
7	Carnegie Mellon	0.11	UIUC	1.18	UIUC	0.77
8	Purdue	0.11	Washington	1.13	UCLA	0.75
9	USC	0.11	U Michigan	1.12	Wisconsin-Madison	0.74
10	U of Georgia	0.11	UCLA	1.09	U Michigan	0.66

In Fig. SM3, we illustrate the effect of ω on the authority supracentralities with a layer-teleportation parameter of $\gamma = 10^{-2}$. In panels (a) and (b), we show the layers' MLC and nodes' MNC, respectively. We observe three qualitative regimes: weak, intermediate, and strong coupling. The insets in (a) and (b) compare observed conditional node centralities

for $\omega = 1$ and $\omega = 10^4$, respectively, to the asymptotic values given by Thms. 4.2 and 4.7, respectively.

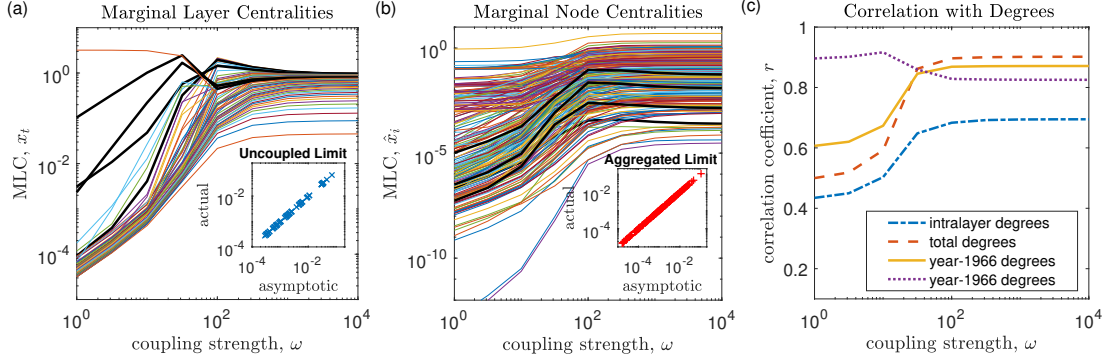


Figure SM3. Supracentrality analysis of the Ph.D. exchange network with the layers' centrality matrices given by their authority matrices and the interlayer adjacency matrix given by Eq. (5.5) in the main text with layer-teleportation parameter $\gamma = 10^{-2}$. (a) MLCs versus ω . (b) MNCs versus ω . The insets in (a) and (b) compare observed conditional node centralities for $\omega = 1$ and $\omega = 10^4$, respectively, to the asymptotic values given by Thms. 4.2 and 4.7, respectively. (c) Pearson correlation measuring the similarity between supracentralities and the node degrees (see the text).

In Fig. SM3(c), we plot (as a function of ω) the Pearson correlation coefficient r between node degrees and supracentralities for three cases: total degrees $\{\bar{d}_i\}$ and conditional node centralities, averaged across layers; intralayer degrees (i.e., $d_i^{(t)} = \sum_j A_{ij}^{(t)}$) and conditional centralities; and degrees in layer $t = 1966$, (i.e., $d_i^{(1966)} = \sum_j A_{ij}^{(1966)}$) and conditional centralities, again averaged across the layers. The gold dashed curve indicates the Pearson correlation coefficient between the marginal-node centralities and the values $\sum_j C_{ij}^{(1966)} = \sum_{k,j} A_{ki}^{(1966)} A_{kj}^{(1966)}$, which give a first-order approximation to the authority scores for the dominant layer ($t = 1966$). (See footnote 3 on page 18 of the main text.) Note for very large values of ω , the authority supracentralities correlate strongly with the nodes' total degrees. However, for very small values of ω the supracentralities correlate strongly with the row summations of the matrices $\mathbf{A}^{(1966)}$ and $\mathbf{C}^{(1966)}$ for layer $t = 1966$, for which the spectral radii of these matrices are larger than the spectral radii of the matrices that are associated with the other layers.